Rate Constants For $H + O_2 + M \rightarrow HO_2 + M$ in Seven Bath Gases

J. V. Michael,* M.-C. Su,† J. W. Sutherland,‡ J. J. Carroll,§ and A. F. Wagner*

Chemistry Division, Argonne National Laboratory, Argonne, Illinois 60439

Received: January 25, 2002; In Final Form: March 21, 2002

The third-order reaction, $H + O_2 + M \rightarrow HO_2 + M$, has been measured near the low-pressure limit at room temperature for M = He, Ne, Ar, Kr, O_2, N_2, and H_2O and over an extended range of temperatures in a shock tube for M = Ar, O_2, and N_2. In all cases, H atoms were produced by the laser photolysis of NH_3 and detected by atomic resonance absorption spectroscopy. The measurements are consistent with the available experimental record and, in particular, confirm the exceptionally high recombination rate constant when M = H_2O. The standard theoretical analysis is applied to this entire experimental record to derive the value of the average energy change per collision, $-\Delta E_{all}$. The resulting $-\Delta E_{all}$ values are sensible for all M but H_2O. The problem with H_2O motivates a change in the standard theoretical analysis that both rationalizes the behavior of H_2O and also quantitatively changes the derived $-\Delta E_{all}$ values for the other species of M. These changes involve three modifications of the standard treatment: (1) explicit temperature dependence in the number of active rotational degrees of freedom contributing to the HO_2* state density, (2) the replacement of Lennard-Jones potential for the HO_2* + M interaction with an electrostatic + dispersion potential, and (3) the calculation of the collision rate between HO_2* + M by a free rotor model for "complex formation" between the M and HO_2*. The optimized values of $-\Delta E_{all}$ that are produced from this new analysis have the following characteristics: (1) the value of $-\Delta E_{all}$ is the same for all rare gases, and (2) $-\Delta E_{all}$ for di- and polyatomic molecules are enhanced relative to the rare gas atoms. This work supports the conclusions of previous trajectory studies that collision rates between activated complexes and bath gases are often underestimated while $-\Delta E_{all}$ derived from recombination kinetics measurements are often overestimated.

Introduction

The third-order reaction, $H + O_2 + M \rightarrow HO_2 + M$, is important as a chain terminating reaction in combustion. The reaction competes with the branching reaction, $H + O_2 \rightarrow OH + O$, at temperatures less than ~900 K and, therefore, has a substantial effect in the later stages of combustion in both flames and practical combustors.[1] It is also important in atmospheric chemistry and converts free H-atoms to the relatively stable radical, HO_2, which interacts in the HO_x atmospheric reaction cycle.[2] Rate constants for the title reaction have therefore been the subject of numerous experimental studies.[3] Even though there have been numerous studies that may or may not have included theoretical descriptions, systematic studies, involving a substantial number of bath gases, are relatively rare. This supplies the motivation for the present work. We have measured room temperature rate constants in seven bath gases. We additionally have measured the temperature dependence of the rate behavior in three of these gases. All of the results are then theoretically discussed using the well-known formalism of Troe and co-workers.[4−8]

* Corresponding author. Address: D-193, Bldg. 200, Argonne National Laboratory, Argonne, IL 60439. Phone: (630) 252-3171. Fax: (630) 252-4470. E-mail: Michael@anlchm.chm.anl.gov.

† Faculty Research Participant, Department of Educational Programs, Argonne. Permanent address: Department of Chemistry, Butler University, Indianapolis, IN 46208.

‡ Present address: Guest Scientist, Department of Energy Sciences and Technology, Brookhaven National Laboratory, Upton, NY 11973.

§ Faculty Research Participant, Department of Educational Programs, Argonne. Permanent address: Department of Chemistry, Drew University, Madison, NJ 07940.

Experimental Section

Apparatus. The experiments have been performed using a laser photolysis-shock tube (LP−ST) apparatus that has been previously described.[9−11] Two types of experiments are reported. Data have been obtained at room temperature, and in this instance, the shock tube served simply as a static reaction vessel. However, the database with N_2, O_2, and Ar diluents has been extended to higher temperatures in reflected shock tube experiments using the LP−ST technique. In both types of experiments, the tube was routinely pumped between experiments to less than 10^{-8} Torr by an Edwards Vacuum Products Model CR100P packaged pumping system. A Questek 2860 ArF excimer laser supplied a photolysis pulse (193 nm, ~25 ns) that entered the tube axially through a Suprasil window on the end plate. The H-atom source molecule in all experiments was NH_3 at concentrations not exceeding 1.2×10^{14} molecules cm^{-3}. H-atoms were formed on photolysis from $NH_3 + h\nu \rightarrow NH_2 + H$, and the laser energy was regulated so that $[H]_0 \cong 1 \times 10^{12}$ atoms cm^{-3} at the photometer position, 6 cm from the end plate. Therefore, subsequent reactions of H with NH_3 and/or NH_2 or NH_2 with O_2[12] were entirely negligible under all of the present conditions. This was confirmed by carrying out experiments with no added reactant (O_2 in this work). Also, at this level of sensitivity, simulations showed that perturbations due to secondary reactions (e.g., $H + HO_2$) were $<+2\%$ and are likewise negligible within experimental error. The only atomic depletion observed was a very minor but measurable decay at higher temperatures and/or very low pressures due to diffusional loss from the viewing zone.

10.1021/jp020229w CCC: $22.00
Published on Web 05/02/2002

The H-atom detection technique was atomic resonance absorption spectrometry (ARAS) using a Gaussian line shape[13,14] from a microwave driven discharge lamp. The absorption path length was 4.2 ± 0.2 cm, and the resonance lamp beam was detected by an EMR G14 solar blind photomultiplier tube. A 4094C Nicolet digital oscilloscope recorded the raw data signals. MgF_2 lenses (cutoff 110 nm) were used in the photometer optics. Since some nonresonant radiation is present in the lamp, an atomic filter section was placed in front of the lamp in order to determine the fraction of the signal that was Lyman-α. This filter section was a fast discharge flow system containing 0.2 Torr H_2, which yielded sufficient H-atoms in the optical path so as to absorb all resonance radiation.[13,14] This filter section measurement was made before each experiment. It was then turned off during the kinetics runs.

Room-Temperature Experiments. Most of the room-temperature experiments have been carried out in excess diluents, N_2, Ar, Kr, Ne, and He, with ppm levels of NH_3 (used as the H-atom source) and ∼1−2% of O_2 also added. The rate of H-atom decay was adjusted to be ≤25 000 s^{-1} by varying total pressure, and typical total pressures then ranged from ∼25 to 200 Torr depending on bath gas. In the H + O_2 + O_2 case, the rate is quadratically dependent on O_2, and the maximum pressure in these experiments had to be limited to no more than 30 Torr. The determination with H_2O as the bath gas was more difficult. For these experiments, two H_2O/O_2 mixtures have been used at relatively low pressures. With ∼15% H_2O to 85% O_2, experiments could be carried out between 2.2 and 3.0 Torr. The pressure range could be slightly extended to 7.0 Torr with ∼9% H_2O to 91% O_2. Both sets required substantial corrections to the first-order H-atom decays (1) from diffusional loss from the viewing zone and (2) from depletion due to H + O_2 + O_2, with (2) being the most important. Hence, these experiments are by far the least accurate reported in the work.

LP−ST Experiments. The LP−ST technique has already been described in detail.[9−11] The shock tube consists of a 7 m (o.d. 4 in.) stainless steel tube separated from a driver section by a thin aluminum diaphragm (4 mil). Shock velocities are measured by equally spaced fast pressure transducers, and the thermodynamic conditions in the reflected shock regime are calculated from the incident shock Mach number.[9,15,16]

Reflected shock wave experiments were carried out in three diluents, Ar, N_2, or O_2, where the gas is effectively stagnant. In the Ar and N_2 experiments, the reactant gas mixture was mostly diluent with 2.0−2.5% added O_2 depending on the loading pressure (i.e., 30, 40, or 50 Torr). The mole fraction of NH_3 was varied so that $[NH_3]_0 \leq 5 \times 10^{13}$ molecules cm^{-3} under reflected shock wave conditions. Low-pressure experiments with O_2 as the third-body were carried out in neat O_2 with varying loading pressures between 4 and 8.0 Torr. Experiments with ∼50% each of O_2 and Ar have also been performed between 8 and 16.0 Torr loading pressure, and these required corrections due to the concurrent process, H + O_2 + Ar. In these latter experiments the mole fraction of NH_3 was again varied so that $[NH_3]_0 \leq 1 \times 10^{14}$ molecules cm^{-3} under reflected shock wave conditions.

Gases. High-purity He (99.995%), used as the driver gas, was from AGA Gases. Ar, O_2, and N_2 were obtained from MG Industries, all being Scientific Grade (99.9999, 99.999, and 99.996%, respectively), and were used without further purification. Ultrahigh-purity grade He (99.999%) for the resonance lamp and experimental mixtures and high-purity H_2 (99.995%) for the atomic filter were from AGA Gases. Ne and Kr were Scientific Grade (both being 99.999%) were from Spectra Gases, Inc. and were used without further purification. Deionized H_2O and NH_3 were both purified by bulb-to-bulb distillation in a greaseless, all-glass, high-vacuum gas handling system retaining the middle thirds. The experimental mixtures were accurately prepared from pressure measurements using a Baratron capacitance manometer and were stored in an all glass vacuum line.

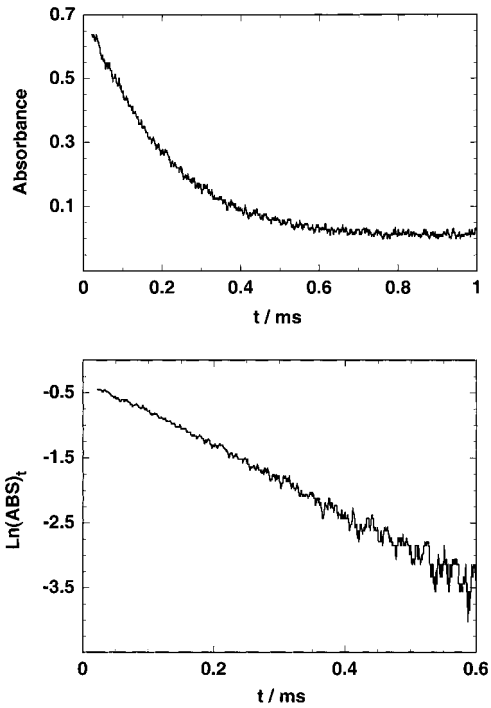

Figure 1. Top panel shows a typical H-atom ARAS absorbance record in an H + O_2 + O_2 experiment at room temperature: $T = 296$ K, $\rho = 4.133 \times 10^{17}$ cm^{-3}, $[O_2]_0 = 3.923 \times 10^{17}$ cm^{-3}, and $[NH_3]_0 = 2.303 \times 10^{14}$ cm^{-3} (see text). The bottom panel shows the corresponding $\ln(ABS)_t$ profile. A linear-least-squares analysis yields the pseudo-first-order decay constant $k_{first} = 5240$ s^{-1}.

Results

For the range of [H] used in these experiments, Beer's law is valid,[13,14] and, therefore, $[H]_t = (ABS)_t/\sigma l$, where $(ABS)_t \equiv \ln(I_t/I_0)$ (I_t and I_0 refer to time-dependent and incident photometric intensities, respectively, σ is the effective atomic cross section, and l is the absorption path length). Since $[H]_t$ is proportional to $(ABS)_t$, it is necessary to only measure relative changes in absorbance. After photolytic formation from NH_3, H-atoms are removed by H + O_2 + M under conditions where both $[O_2]$ and [M] are effectively constant. [H] can also be removed by pseudo-first-order diffusion out of the viewing zone under high temperature and/or low-pressure conditions. Hence, $d[H]/dt = -(k_{ter}[O_2][M] + k_d)[H]$ gives the rate law

$$\ln(ABS)_t = -(k_{ter}[O_2][M] + k_d)t + C \qquad (1)$$

and plots of ln(ABS) against time give the first-order decay constants, k_{first}, which are equal to $k_{ter}[O_2]_0[M]_0 + k_d$. If more than one diluent is present, the equation then becomes, $k_{first} = \sum_i k_{ter\ i}[M]_{0i}[O_2]_0 + k_d$. In most of the present experiments at 296 K, the diffusion correction was negligible, and therefore, an apparent bimolecular rate constant was then determined as $k_{bi} = k_{first}/[O_2]_0$, and these are then plotted against [M] to yield k_{ter}.

Figure 1 shows a typical example with O_2 alone as the diluent. The top panel shows the measured H-atom ARAS absorbance decrease in an experiment at 12.67 Torr at 296 K. The bottom

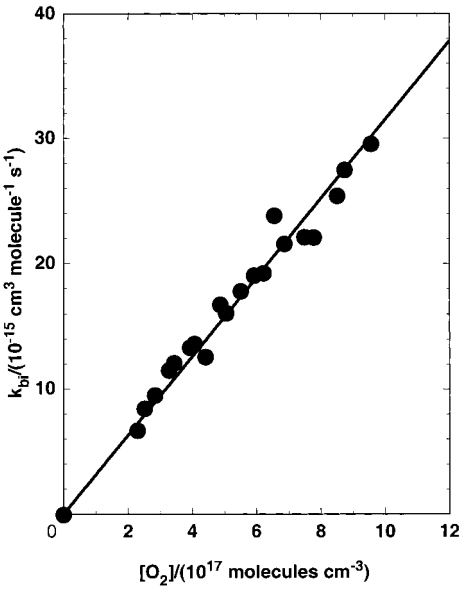

Figure 2. Plot of apparent bimolecular rate constants for $H + O_2$ at room temperature against $[O_2]$. The solid line is the linear-least-squares fit of the experiment data which gives a slope, $k_{ter} = (3.14 \pm 0.06) \times 10^{-32}$ cm^6 molecule^{-2} s^{-1} (see text).

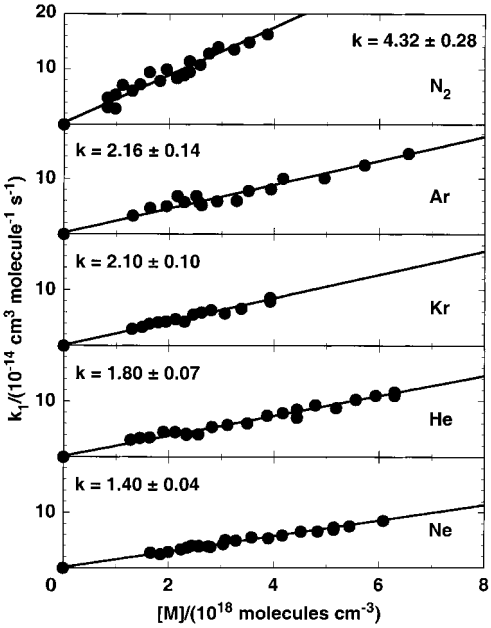

Figure 3. Combined graph of room-temperature $H + O_2$ bimolecular rate constants as a function of [M] (M = N_2, Ar, Kr, He, and Ne). Each of the inserted k values is k_{ter}, in units of 10^{-32} cm^6 molecule^{-2} s^{-1} for the respective M derived from a linear-least-squares fit of the corresponding experiment data.

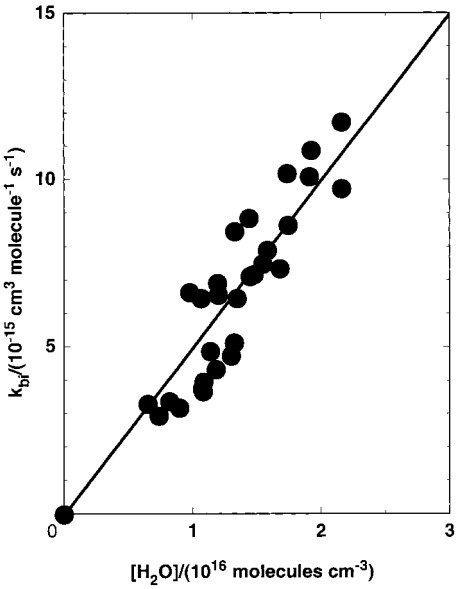

Figure 4. Plot of $H + O_2$ bimolecular rate constants at room temperature against $[H_2O]$. The linear-least-squares fit gives $k_{ter} = (5.0 \pm 0.5) \times 10^{-31}$ cm^6 molecule^{-2} s^{-1} for H_2O bath gas.

panel shows the pseudo-first-order plot, which gives, according to eq 1, a value for k_{first} from the negative slope. k_{bi} can then be calculated by $[O_2]_0$ division into k_{first}. Twenty-one additional experiments were performed with varying total pressures, and the resultant k_{bi} values are subsequently plotted against $[O_2]$ in Figure 2. The (0, 0) constrained line from this plot then gives the room-temperature value for the termolecular reaction, $H + O_2 + O_2$, as $k_{ter}^{O_2} = (3.14 \pm 0.06) \times 10^{-32}$ cm^6 molecule^{-2} s^{-1}, where the error is two standard deviations.

About 20 similar experiments have been carried out each with N_2, Ar, Kr, He, and Ne as third-bodies. The results of these experiments are shown in Figure 3 as graphs of k_{bi} against [M]. The (0, 0) constrained lines are also shown, and the slopes give respective k_{ter} values: 4.32 ± 0.28, 2.16 ± 0.14, 2.10 ± 0.10, 1.80 ± 0.07, and 1.40 ± 0.04, all in units of 10^{-32} cm^6 molecule^{-2} s^{-1}. The indicated errors are two standard deviations. As indicated above, experiments have also been performed with H_2O as the third-body. These experiments had to be carried out at low pressure and with substantial quantities of added O_2. Hence, first-order-decay constants are then $k_{first} = k_{ter}^{O_2}[O_2][O_2] + k_{ter}^{H_2O}[H_2O][O_2] + k_d$. k_d values were measured in low-pressure NH_3/N_2 experiments, and these were assumed to be appropriate for O_2 as third-body. Corrections from diffusion were significant but not nearly as important as corrections from the concurrent $H + O_2 + O_2$ reaction. $k_{bi}^{H_2O} = k_{ter}^{H_2O}[H_2O]$ is then evaluated as $(k_{first} - k_d)/[O_2] - k_{ter}^{O_2}[O_2]$. These residual values were then plotted against $[H_2O]$, as shown in Figure 4. Because the fractional decay due to $H + O_2 + O_2$ is substantial, the plot shows scatter. Even so, there is a clear trend in the data which can be expressed by the (0, 0) constrained line giving $k_{ter}^{H_2O} = (50 \pm 5) \times 10^{-32}$ cm^6 molecule^{-2} s^{-1}. This result shows that $k_{ter}^{H_2O}$ is ~23 times larger than k_{ter}^{Ar} at 296 K.

Experiments at higher temperatures in three third-bodies (N_2, Ar, and O_2) have been carried out using the LP−ST technique. These experiments required small corrections due to diffusion, and these were directly measured in NH_3/N_2 and NH_3/Ar mixtures. The values measured in the former mixture were used for the O_2 experiments in exactly the same way as at room temperature. However, the major $[H]_t$ depletion process in all cases is the title reaction. The experimental analyses are the same as that shown in the room temperature illustration of Figure 1; however, the thermodynamic conditions behind the reflected shock waves were determined as described previously[15,16] from a knowledge of incident shock velocities. In this case, the evaluated termolecular rate constants, k_{ter}^{M}, were calculated as $(k_{first} - k_d)/[M][O_2]$. Fifteen values in N_2 over the T range 471−698 K were measured. Twenty-one values in Ar (482−712 K) and twenty-five values in O_2 (513−697 K) were similarly obtained, and all three databases were combined with the present values at 296 K. Since the database at room temperature is much more extensive, these values were given ~20 times more weight in a statistical analysis based on the T-dependent equation, $k(T) = AT^n$, and its logarithmic form, $\ln k(T) = \ln A + n \ln T$.

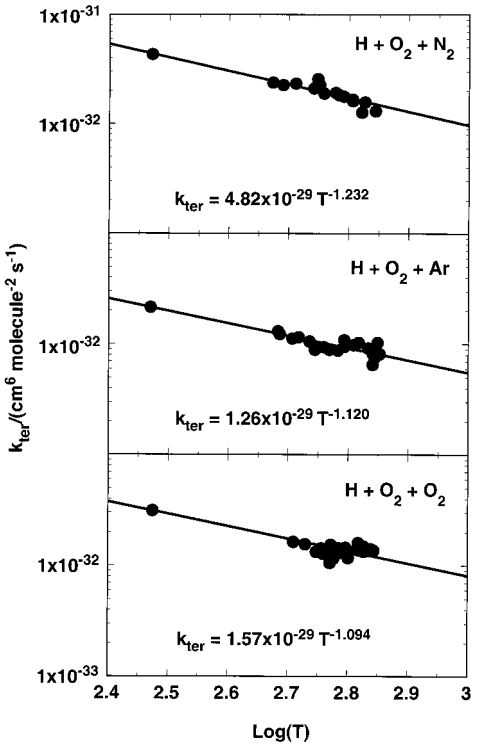

Figure 5. $\log(k_{ter})$ against $\log(T)$ plots for $H + O_2 + M$, $M = N_2$, Ar, and O_2, respectively. The linear-least-squares lines, for each case, are derived from the experimental data within the temperature range specified in the text.

The data for the three cases are plotted in Figure 5 along with linear-least-squares lines based on this equation. The results can be summarized as

$$k_{ter}^{N_2}(T) = (4.82 \pm 1.03) \times 10^{-29} T^{-1.232 \pm 0.036} \text{ cm}^6 \text{ molecule}^{-2} \text{ s}^{-1} \quad (2)$$

$$k_{ter}^{Ar}(T) = (1.26 \pm 0.27) \times 10^{-29} T^{-1.120 \pm 0.035} \text{ cm}^6 \text{ molecule}^{-2} \text{ s}^{-1} \quad (3)$$

and

$$k_{ter}^{O_2}(T) = (1.57 \pm 0.38) \times 10^{-29} T^{-1.094 \pm 0.040} \text{ cm}^6 \text{ molecule}^{-2} \text{ s}^{-1} \quad (4)$$

Hence, the present results are accurate to within $\sim\pm 20-25\%$ over the temperature range 296 to $\sim$700 K.

Discussion

The present room-temperature results are compared to earlier studies in Table 1.[17−26] Earlier results on two bath gases, H_2 and CH_4, that are not represented in the measurements here are also included in the table. The results from Kurylo,[17] Wong and Davis,[18] Carleton et al.,[19] Hikida et al.,[22] Hack et al.,[24] and Nielsen et al.[26] were carried out under chemical isolation conditions similar to those in the present study. Agreement is generally satisfactory within combined experimental errors. In contrast, the present values are mostly lower than those reported by Cobos et al.,[20] Hsu et al.,[21] Westenberg and deHaas,[23] and Clyne and Thrush.[25] These four studies, indicated in brackets in the table, required substantial chemical modeling in order to extract the rate constants for the title reactions and are therefore less direct.

TABLE 1: Measured Room-Temperature Rate Constants for $H + O_2 + M$

bath gas	$k_{ter}/(10^{-32}$ cm^6 molecule^{-2} s$^{-1})$	reference
N_2	5.3 ± 0.8	Kurylo[17]
	5.5 ± 0.7	Wong and Davis[18]
	4.6 ± 0.3	Carleton et al.[19]
	4.3 ± 0.3	present work
	$[6.5 \pm 1.0]$	Cobos et al.[20]
	$[6.0 \pm 0.8]$	Hsu et al.[21]
Ar	1.6 ± 0.2	Hikida et al.[22]
	1.6 ± 0.2	Kurylo[17]
	2.0 ± 0.2	Wong and Davis[18]
	2.1 ± 0.2	Carleton et al.[19]
	2.2 ± 0.1	present work
	$[1.9 \pm 0.3]$	Westenberg and deHaas[23]
	$[2.8 \pm 0.4]$	Cobos et al.[20]
	$[2.2 \pm 0.2]$	Clyne and Thrush[25]
Kr	2.1 ± 0.1	present work
He	1.6 ± 0.2	Kurylo[17]
	1.9 ± 0.2	Wong and Davis[18]
	2.5 ± 0.3	Hack et al.[24]
	1.8 ± 0.1	present work
	$[2.2 \pm 0.2]$	Clyne and Thrush[25]
	$[2.6 \pm 0.3]$	Hsu et al.[21]
Ne	1.4 ± 0.1	present work
O_2	3.1 ± 0.1	present work
H_2O	50 ± 5	present work
	$[58 \pm 23]$	Clyne and Thrush[25]
	$[64 \pm 12]$	Hsu et al.[21]
H_2	5.9 ± 1.2	Wong and Davis[18]
	4.7 ± 0.6	Hikida et al.[22]
	6.0 ± 0.6	Nielsen et al.[26]
CH_4	42.0 ± 18.3	Wong and Davis[18]
	24.1 ± 3.1	Kurylo[17]
	$[15.0 \pm 2.3]$	Cobos et al.[20]

The most striking feature in the Table 1 results are those with H_2O as the third-body. The present result agrees with the derived values from Hsu et al.[21] and Clyne and Thrush[25] and, when compared to $k_{ter}^{N_2}$ and k_{ter}^{Ar}, give ratios of 11.6 and 23, respectively. Carleton et al.[19] have also determined rate constants at higher temperatures, and their H_2O to N_2 ratio at 580 K is 10.9. In shock tube experiments between 1300 and 1900 K, Getzinger and Blair report an H_2O to Ar ratio of 25.[27] More recent results by Hanson and Bowman and co-workers[28,29] indicate a similar enhancement of the rate constant, giving an H_2O to Ar ratio of 18. These results show that the relative rate constants are not strongly dependent on temperature. Hsu et al.[21] recognized the theoretical significance when Troe's limiting low-pressure rate theory[4,5] was applied to their H_2O data. This theory is applicable to the energy transfer mechanism where the initially formed species is the vibrationally excited adduct, HO_2*, which can be thermally stabilized by collision with the bath gas. Using the Cobos et al.[20] value for $F_{rot} = 9.1$, they found collisional deactivation efficiencies, $\beta_c(He) = 0.15$, $\beta_c(N_2) = 0.34$, and $\beta_c(H_2O) \cong 3$; i.e., with H_2O, an unphysical value substantially greater than unity when the usual Lennard-Jones model[30] was used for calculating collision rates. Total quantum mechanical scattering cross sections for centrosymmetric r^{-6} or r^{-3} potentials were suggested as an alternative, and this method gave $\beta_c(H_2O)$ values that were sensible. In later work,[31] the procedure was further discussed and tested; however, the method has not been widely accepted. Instead, the Lennard-Jones model for calculating collision rates has continued to be used by most workers. Toward the end of this article, we will comment more on the pioneering work of Hsu et al.[21] and Durant and Kaufman.[31]

The calculation of collision rates with the simple Lennard-Jones model continues to be one of the assumptions of the energy transfer mechanism that is used in RRK, RRKM, and

TABLE 2: Parameters for Calculating $k_{ter,sc}$ with the BP Model (Details in Text)

	parameters		
species	$(\epsilon_{1,2}/k)$/K	$\sigma_{1,2}$/Å	T/K
(H, O_2)	24.8	3.348	
(HO_2, He)	61.3	3.004	
(HO_2, Ne)	125.8	3.079	
(HO_2, Ar)	227.2	3.369	
(HO_2, Kr)	260.5	3.476	
(HO_2, H_2)	91.7	3.213	
(HO_2, O_2)	209.6	3.397	
(HO_2, N_2)	187.8	3.519	
(HO_2, CH_4)	231.2	3.550	
(HO_2, H_2O)	768.9	2.873	300
	622.2	2.924	500
	522.3	2.967	1000

species	freq/(cm^{-1})	mom. of inertia/(10^{-39} g cm^2)	E_0/(kcal mol^{-1})
HO_2	3436	0.1375	47.634
	1392	2.503	
	1098	2.650	
O_2	1580	1.936	

	$\log(I^+/I)$	$r(T)$
HO_2*	$0.984 + 0.201(\log T) - 0.0757(\log T)^2$ ±0.4% fitting error (200−1800 K)	$0.4758T^{0.1772}$ ±0.5% fitting error (200−1800 K)

	k_d^∞/s^{-1}	K_c/(molecules cm^{-3})
$HO_2 \leftrightarrow H + O_2$	$4.470 \times 10^{12}T^{0.5468}e^{-24209K/T}$ ±4% fitting error (200−1800 K)	$4.689 \times 10^{22}T^{0.3599}e^{-24163K/T}$ ±5% fitting error (200−1600 K)

Troe's theory for low-pressure limits. In the present work, we follow the spirit of Hsu et al.[21] and Durant and Kaufman[31] by first applying Troe's limiting low-pressure rate theory, with a Lennard-Jones model based on the most recent determination of effective Lennard-Jones parameters. This method has been shown to give theoretical predictions that are quite similar to those from Gorin/RRKM or ab initio/RRKM approaches for a variety of atom with radical reactions.[32] We will then consider non-Lennard-Jones electrostatic potentials, that are ultimately incorporated into a trajectory-validated method, for collisional deactivation of chemically activated small polyatomic molecules. In the following sections, the Troe theory will be briefly reviewed. The collision rate for that theory will be evaluated and discussed with a Lennard-Jones description of the interaction potential. Then different formulations of the collision rate and more accurate formulations of the interaction potential will be examined. Finally, the comparison between theory and experiment will be developed.

A. Troe Theory. The strong collision low-pressure bimolecular limiting rate constants for dissociation of HO_2 are calculated according to Troe[4,8] from

$$k_{d,sc} = Z_{coll}(\rho_{vib}RT/Q_{vib})F_{anh}F_E F_{rot}e^{-E_0/RT} \qquad (5)$$

and the strong collision termolecular rate constants are determined from $k_{ter,sc} = k_{d,sc}K_c^{-1}$ where K_c is the equilibrium constant for $HO_2 \rightleftharpoons H + O_2$. Each of the quantities in eq 5 will be discussed below. β_c is the value that is necessary to make theory agree with experiment, i.e., $\beta_c = k_{ter,exp}/k_{ter,sc}$. β_c has the physical interpretation of being the inverse of the number of collisions between the activated molecule, HO_2*, and the buffer gas that stabilizes the activated species. A fractional value of β_c contains information on the average energy transfer per collision of the activated molecule with the buffer gas. However, a value of β_c larger than unity implies that the activated complex is stabilized faster than the collision rate, and this is an unphysical result.

To apply eq 5, values of F_E, F_{anh}, and F_{rot} have to be determined. The molecular properties necessary to do the evaluation are given in Table 2. Even though F_E is nearly unity, it was evaluated from the formula given by Troe.[4] Ambiguities in the product $F_{anh}\rho_{vib}$ were eliminated by using the quantum mechanical scattering results from Dobbyn et al.,[33] who used the DMBE IV potential energy surface from Pastrana et al.[34] These workers found that the number of states at threshold was 320. The well depth of the Pastrana et al. surface is $V = 54651$ giving $E_0 = 46\,180$ cal mol^{-1}. From Litorja and Ruscic,[35] $E_0 = 47\,634$ cal mol^{-1}; hence, we have used the Whitten−Rabinovitch formula[36] with this E_0 change to modify the total state count, obtaining 346. The harmonic Whitten−Rabinovitch count is 237. Hence, we accounted for this difference by simply considering F_{anh} to be the ratio, i.e., 1.46. This factor also adjusts the Whitten−Rabinovitch vibrational state density giving $F_{anh}\rho_{vib} = 0.0531/cm^{-1}$ at threshold to be compared to Troe's estimate of $0.064/cm^{-1}$.[8] Use of the newer potential surface of Harding et al.[37] will not appreciably affect the state count estimate since the differences between this surface and DMBE IV[34] are subtle.[38] Using dynamical arguments, Waage and Rabinovitch derived an expression for F_{rot},[39]

$$F_{rot} \cong F_{rot,max}\left[\frac{I^+/I}{I^+/I - 1 + F_{rot,max}}\right] \qquad (6)$$

and this has been adopted by Troe.[4−8] I^+/I is the ratio of the moment of inertia for the activated complex to that moment in HO_2 that correlates to I^+ in the complex. From Table 2, the I for H rotation around the axis specified by the O−O bond (i.e., 1.375×10^{-40} g cm^2) will be associated with a loose H−O_2 complex. As in past work,[32] a Lennard-Jones complex for H with O_2 (Table 2) will be taken to be the activated complex. Consequently, a pseudo-diatomic calculation for I^+ is sufficient in which case $I^+ = \mu_{H,O_2}r^2$, where $r = \sigma_{H,O_2}(\Omega^{22}\bigstar_{H,O_2})^{1/2}$. The collision integral[30] is necessary because it compensates for conservation of angular momentum in the collision process. The

values of the ratio are therefore *T*-dependent since the effective distance between H and O_2 in the complex decreases with increasing temperature. Using the values from Table 2, we find for $200 \le T \le 1800$ K (to within ±0.4%) that $\log(I^+/I) = 0.984 + 0.201(\log T) - 0.0757(\log T)^2$. This gives $I^+/I(300\text{ K}) = 10.4$ to be compared to 9.1 from Cobos et al.[20] and 10.4 from Troe.[8] At 1500 K Troe reports[8] $I^+/I = 5.7$ whereas the present model gives 7.2, showing that the two different approaches give similar results. $F_{rot,max}$ in eq 6 comes from contributing rotations where ρ_{vib} and Q_{vib} in eq 5 are replaced by $\rho_{r,vib}$ and $Q_{r,vib}$ in which case $F_{rot} \equiv (\rho_{r,vib}Q_{vib}/\rho_{vib}Q_{r,vib})$. Using the Whitten−Rabinovitch expressions,[36] the explicit formula for F_{rot} then becomes

$$F_{rot} = \frac{(s + r/2)\Gamma(s)}{\Gamma(s + 1 + r/2)}\left(\frac{E_0 + aE_z}{RT}\right)^{r/2} \qquad (7)$$

where *r* is the number of active rotations. For the special case, $r = 3$, F_{rot} is $F_{rot,max}$.[4−8] We have then evaluated F_{rot} from eq 6 with $F_{rot,max}$ from (7) and our derived I^+/I values. F_{rot} values at 300 and 1500 K of 9.8 and 5.0 are obtained and can be compared to respective values from Troe[8] of 9.8 and 4.2, showing again that the approaches are quite similar.

Equation 6 is based on dynamical considerations[39] whereas eq 7 is directly derived[36] from an harmonic oscillator-rigid rotator model for state densities and counts for the case of *r* contributing rotations. If the present F_{rot} values from (6) are compared to those from (7) with $r = 1$, 2, or 3, the range falls between 1 and 2 active rotations. Hence, the implication of the dynamical model is that, on average, one or more rotations become active in HO_2 and have to be considered when assessing the total state density at threshold. In fact, equating eqs 6 and 7 over the *T* range 200−1800 K, with *r* being the parameter, shows that *r* varies from 1.217 at 200 K to 1.796 at 1800 K; i.e., the effective number of active rotational degrees of freedom is *T*-dependent. We find to within ±0.5% that $r(T) = 0.4758T^{0.1772}$, as listed in Table 2.

Accepting that $r(T)$ overall rotations are active in HO_2, the description of the HO_2* part of eq 5 is now complete and cannot be changed as a function of the third-body M. The consequence of having $r(T)$ overall rotations being active is that some pressure dependence in the rate constants is to be expected particularly when assessing weak collisional effects.[6,7]

The M dependence in the low-pressure limit is contained in the collision rate, Z_{coll}, the only remaining quantity in eq 5 that has not yet been determined. However, an extended discussion of the determination of Z_{coll} will be facilitated by first reviewing the Troe approach for handling the pressure dependence in the experimental data. This approach requires only the low- and high-pressure limits to the recombination rate. Equation 5 concerns only the low-pressure limit as mentioned above. The high-pressure limiting rate constant for H + O_2 (i.e., $k^\infty_{H+O_2}$) can be calculated for an activated complex taken to be a Lennard-Jones complex. This method has been used previously[32] in our laboratory for atom with molecule adducts and gives estimates that are generally ∼60−70% of those obtained using more fundamental variational transition state theory on well-defined ab initio potential energy surfaces.[32] When applied to H + O_2 with modern estimates[40,41] of the Lennard-Jones parameters (see Table 2), the results give $k^\infty_{H+O_2}$ between 2.05 and 3.81×10^{-10} cm^3 molecule^{-1} s^{-1} (200−1800 K). From classical trajectory calculations, $k^\infty_{H+O_2}$ has recently been estimated at $(0.96-1.79) \times 10^{-10}$ cm^3 molecule^{-1} s^{-1} between 300 and 1325 K,[3] i.e., a factor of ∼2.2 smaller than the present estimate. Since almost all measurements are near the low-pressure limit, this smaller value has relatively little effect on the predictions. For example, with Ar at 1 atm or below, the predictions are the same to within <3%. Much of the data above 1 atm were obtained at temperatures greater than ∼1000 K, and for these data, the discrepancy with the lower estimate at 1300 K is still <3%; i.e., the predictions are not strongly dependent on $k^\infty_{H+O_2}$. With our higher value for $k^\infty_{H+O_2}$, we can adequately fit the room-temperature pressure dependent data of Cobos et al.[20] up to ∼5 bar, after which our values become increasingly larger than measured. Hippler et al.[42] have shown in the O + NO + M case that neglect of diffusional effects above 5−10 bar can result in an experimental underestimate of the high-pressure rate constant. Such an effect may be operative in H + O_2 + M also leading to an underestimated value for $k^\infty_{H+O_2}$ by Cobos et al.[20] Given the values of $k^\infty_{H+O_2}$, the computed high-pressure limit for dissociaton, k_d^∞, can be fitted by $4.470 \times 10^{12}T^{0.5468}e^{-24209K/T}$ s^{-1} to within ±4% over 200−1600 K (Table 2).

B. Lennard-Jones Model for Collision Rates. The usual expression for the collision rate Z_{coll}, the last remaining quantity in eq 5, is

$$Z_{coll} = \langle v\rangle \pi {\sigma_{12}}^2 \Omega^{22}\bigstar \qquad (8)$$

where $\langle v\rangle$ is the Boltzmann average thermal velocity [$=(8kT/\pi\mu_{12})^{1/2}$] and $\Omega^{22}\bigstar$ is a function of $T^* = kT/\epsilon_{12}$ that can be calculated from the polynomial forms given by Bzowski et al.[40] and/or Paul[41] if the parameters ϵ_{12} (well depth) and σ_{12} (distance at which the potential passes through zero) are interpreted as effective Lennard-Jones parameters. A complete description of the rationale and method for determining effective (ϵ, σ) parameters is given by Bzowski et al. and is further described and extended for use in combustion systems by Paul[41] and Paul and Warnatz.[43] The basic strategy of this approach is to use more realistic representations of the interaction potential, which are then reduced to hopefully superior effective Lennard-Jones parameters from which the standard collision rates can be calculated. The effective Lennard-Jones parameter values for ϵ/k and σ can be obtained using seven molecular parameters (tabulated by Paul[41]) for each species. The method adjusts for both induced dipole−induced dipole and dipole−induced dipole interactions. Methods are also given for calculating dipole−dipole interactions. The method does not take into consideration quadrupole moments. The assumed full potential has $\exp(-r/\rho)$ character at short distances which joins r^{-x} (where $x = 12$, 6, and/or 3) components depending on which species are interacting. However in the end, the actual potential is reduced to an effective Lennard-Jones form. For the rest of this paper, this approach and the ultimate Lennard-Jones potentials produced will be labeled by the acronym "BP".

The BP approach is validated by reproducing measured diffusion and viscosity data of stable molecules and, in some cases, reproducing molecular beam scattering data. However, there is no experimental database of transport properties for two polar species. In fact, Bzowski et al.[40] do not compare their models to measurements for any species involving permanent dipole moments. Paul briefly mentions such comparisons but never specifically mentions the systems or the results.[41] Furthermore, to our knowledge, there are no useful measurements for transport properties between two species which both have dipole moments. Finally, there are no measurements for transport properties of which we are aware that involve molecular radicals, certainly none that involve HO_2. Therefore, while the BP approach can be applied to species with dipole

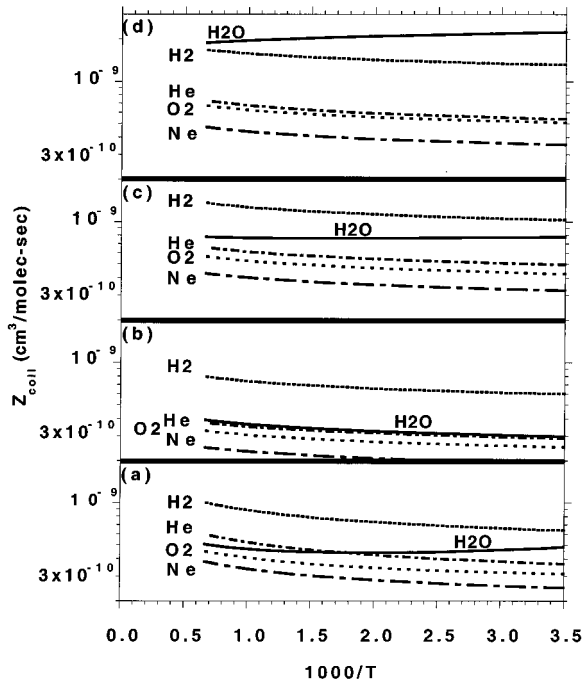

Figure 6. Computed Z_{coll} versus inverse temperature for five different bath gases. The five bath gases are: He (— · —), Ne (— · · —), H_2 (···), O_2 (- - -), and H_2O (—). Each panel represents a different model for Z_{coll} as described in the text.

moments, there is no convincing validation for the approach in such situations.

In the present case, HO_2 has a permanent dipole and polarizability while all other third-bodies except H_2O have no dipole but do have small polarizabilities (and in some cases quadrupole moments which the BP approach will ignore). Hence, for HO_2, the interactions with eight of the nine bath gases listed in Table 2 are dipole−induced dipole. With H_2O the interaction is dipole−dipole. The BP Lennard-Jones parameters for all nine HO_2−M pairs, where M is the bath gas, are listed in Table 2. For the dipole−dipole HO_2−H_2O interaction, BP methodology gives temperature-dependent effective Lennard-Jones parameters. When these are applied to eq 8, the resulting Z_{coll} values as a function of temperature are displayed in panel a of Figure 6 for a representative sample of bath gases. These bath gases include He and Ne, which span the range of Z_{coll} for all other rare gases, H_2 and O_2, which span the range of Z_{coll} covered by the diatomic gases and CH_4 in Table 1, and H_2O, which has the strongest interaction potential with HO_2. Given the wide variation in the strength of the interaction potential, the figure shows a surprisingly tight cluster of Z_{coll} values as a function of M. This clustering is driven by the counteracting trends of higher velocities for lighter M species but larger values of σ and $\Omega^{22}\bigstar$ for heavier M species.

With the computation of Z_{coll}, the determination of the low-pressure limit with eq 5 is complete. With insertion of that limit into the complete Troe theory[4−7] including pressure dependence via incorporation of the computed high-pressure limit discussed above, the predicted rate constants at room temperature for rare gas third-bodies are in satisfactory agreement with experiment if $-\Delta E_{all} = 115$ cal mol^{-1} (40.2 cm^{-1}). This value implies $\beta_c(300\ K) = 0.1227$ for all rare gases and predicts: 2.35, 1.59, 1.98, and 1.97 for He, Ne, Ar, and Kr, respectively, to be compared to 1.80 ± 0.07, 1.40 ± 0.04, 2.16 ± 0.14, and 2.10 ± 0.10, all in units of 10^{-32} cm^6 molecule^{-2} s^{-1}. The largest discrepancy, +31%, is with He bath gas. These results show that the rate behavior in the rare gases scales directly, within experimental error, with Z_{coll} as calculated with eq 8 from the parameters of Table 2 and as displayed in panel a of Figure 6. As pointed out before,[44−46] Z_{coll} is always lowest for Ne. Even though the ϵ/k and σ values for He are lower than for Ne, the relative velocity is higher, resulting in predictions for He that are about the same as with Ar and Kr.

The 300 K results for the two diatomic molecules, O_2 and N_2, require higher values for $-\Delta E_{all}$. With respective values of 195 and 280 cal mol^{-1} (i.e., 68.2 and 97.9 cm^{-1} giving β_c = 0.1832 and 0.2363), the predicted rate constants of 3.11 and 4.32 can be compared to present measured rate constants 3.13 ± 0.06 and 4.32 ± 0.28, all in units of 10^{-32} cm^6 molecule^{-2} s^{-1}. With H_2 bath gas, Wong and Davis,[18] Hikida et al.,[22] and Nielsen et al.[26] report $k_{H+O_2}{}^{H_2}$ as 5.9, 4.7, and 6.0 × 10^{-32}, respectively, and the present calculation gives 5.96 × 10^{-32} cm^6 molecule^{-2} s^{-1} with $-\Delta E_{all} = 195$ cal mol^{-1} (68.2 cm^{-1} giving $\beta_c = 0.1832$). Kurylo[17] and Wong and Davis[18] report values with CH_4 as the bath gas that do not agree. However, Wong and Davis have a large enough uncertainty (±40%) so that the error bars overlap. The value by Cobos et al.,[20] $k_{H+O_2}{}^{CH_4} = 15 \times 10^{-32}$ cm^6 molecule^{-2} s^{-1} has less uncertainty (±15%) and is in better agreement with Kurylo (even though the error bars just avoid overlapping). With $-\Delta E_{all} = 1750$ cal mol^{-1} (612 cm^{-1}) at 300 K ($\beta_c = 0.6168$) the theoretical results can recover the Cobos et al. value.

The theory comparisons presented above have been restricted to dipole−induced dipole interactions as calculated with the BP method. The case with H_2O has therefore not yet been considered. The ϵ/k and σ values for HO_2−H_2O computed by the BP method, when applied to eq 8, give Z_{coll} values so low that they imply $\beta_c(H_2O)$ values substantially greater than unity, particularly at lower temperatures. Our conclusion is the same as already discussed by Hsu et al.[21] and Durant and Kaufman.[31] The origin of the difficulty is quite clear in panel a of Figure 6. Despite being the only dipole−dipole interaction, the Z_{coll} for HO_2−H_2O that results from eq 8 is quite similar to the Z_{coll} for all other HO_2−M combinations. However, as Table 1 shows, the measured recombination rate constant is at least 10 times bigger for HO_2−H_2O that for any other HO_2−M. This results in $\beta_c(H_2O) > 1$.

C. Alternate Models for Collision Rates. The failure of the usual approach for M = H_2O has motivated a systematic examination of Z_{coll}, the only part of the strong collision low-pressure limit of eq 5 that is M dependent. Two pieces of information are required for Z_{coll}: (1) the underlying potential energy surface, and (2), the association of the collision integral $\Omega^{22}\bigstar$ with the collision rate. Each will be examined in turn. Although the problem is restricted only to H_2O bath gas, all bath gases considered here with the usual approach, will be also be reinvestigated.

C.1. Interaction Potentials. If one is interested in the collision rate of a sequence of colliders, M, with a chemically activated species, X, which has a dipole moment, one can compactly represent the sequence of the BP potentials for a given X by plotting the ϵ for each M with respect to the equilibrium distance r_e (=$2^{1/6}\sigma$). Note that if M has a dipole moment, the BP approach derives effective Lennard-Jones parameters that are temperature dependent. Hence in such a case, the (ϵ, r_e) correlation is not a point but has a range corresponding to the temperature range of interest. Figure 7a shows such a plot for X = HO_2 and for all nine M's mentioned above, while Figure 7b (drawn to the same scale) shows the identical M sequence for X = H_2O. The comparison of the two panels in Figure 7 shows that, in all cases, the X−M interaction has substantially

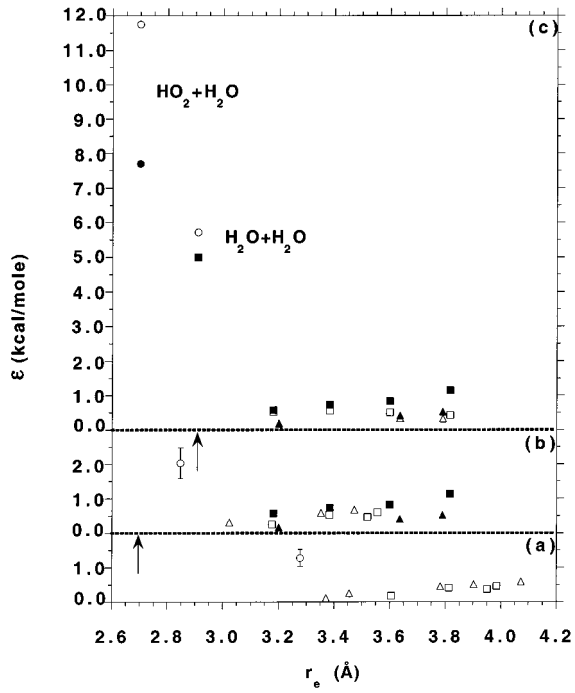

Figure 7. ϵ versus r_e for a sequence of bath gases interacting with HO_2 in (a), H_2O in (b), and both HO_2 and H_2O in (c). In (a), the bath gases for the BP potentials are: H_2O (○); H_2, O_2, N_2, CH_4 (□); and He, Ne, Ar, Kr, Xe (Δ). In this and other panels, when the same symbol is used for a string of bath gases, each bath gas appears from left to right in the panel in the order it appears in the string. In (b), the bath gases for the BP potentials are: H_2O (○); H_2, O_2, N_2, CH_4 (□); and Ne, Ar, Kr (Δ). Except for H_2O, the bath gases for the van der Waals potentials in this panel are the same with solid rather than open symbols. In (c), the bath gases for the van der Waals potentials in (b) are repeated with the addition of H_2O (●) for both HO_2 (as labeled) and H_2O. In (c), the bath gases for the electrostatic potentials are the same as the van der Waals potentials only with solid symbols. The arrows in (a) and (b) are described in the text.

smaller ϵ and longer r_e for X = HO_2 than for X = H_2O. This is a surprising result. The dipole moment and polarizability used in the construction of the BP potential are larger for HO_2 than for H_2O, which would lead to stronger HO_2 interaction potentials. HO_2 is a radical, while H_2O is not, and this would not generally suggest that HO_2 would have the weaker interaction.

Van der Waals information is consistent with this expectation. (The term "van der Waals" will be loosely used here since some of the interactions are more properly termed "hydrogen bonded".) For X = H_2O, there is van der Waals information[47−54] on all of the 9 different M species except M = He. In Figure 7b, this van der Waals information is plotted for all M but He. The van der Waals potential qualitatively obeys the same trends as the BP potentials. However, the van der Waals values for r_e are always larger than those for BP, and the van der Waals ϵ is both smaller, for the rare gases, and larger, for every other M species, than with BP. In Figure 7b, the BP ϵ's for H_2 and N_2 have the largest relative difference with the van der Waals ϵ, approaching underestimations of 40%. However, the largest absolute difference by far is for H_2O where the ϵ value is off scale at 5.0 kcal mol^{-1} at an r_e value indicated by the arrow in the figure. Furthermore, the H_2O-H_2O van der Waals ϵ is one of the most securely known in comparison to those from other van der Waals experiments. For X = HO_2 in Figure 7a, the only available comparison of the BP potential to the van der Waals information is for HO_2-H_2O.[55] The ϵ value is even more off scale at ∼7.7 kcal mol^{-1} at the r_e indicated by the arrow. As the figure shows, not only is the BP ϵ value <20% of the van der Waals value, but the BP r_e value is noticeably larger (not smaller as in Figure 7b) than the van der Waals value. The van der Waals interaction in HO_2-H_2O is computed[55] to be >50% larger than the H_2O-H_2O interaction due to the fact that the extra O-atom makes it possible to form two strong hydrogen bonds instead of one. However, the BP potential basically halves the interaction in going from X = H_2O to X = HO_2.

There is no requirement that an *effective* Lennard-Jones potential should reproduce van der Waals features. Nonetheless, the scale of the discrepancy when M = H_2O and the trend with X strongly suggest that the BP potential underestimates the strength of the HO_2-H_2O interaction. In addition, the largest relative differences of BP ϵ values with van der Waals values occur for those molecules that have the largest permanent moments. This includes the permanent quadrupole moments of H_2 and N_2.

The BP and van der Waals information are closely related only with O_2 (which has a permanent, but weak, quadrupole moment). These trends suggest that permanent moments are strongly reflected in van der Waals informaton but are only weakly reflected in BP potentials. Since there is no validation of BP potentials for transport properties involving two species with permanent moments, this in general suggests that the BP potentials are not fully capturing the effect of permanent moments.

In contrast to BP potentials, it has often been suggested[56] that van der Waals geometries and energies can be largely understood by high-order electrostatics, coupled with effective dispersion forces, and simple models for repulsion due to wave function overlap. This approach results in potentials that are fully dimensional in the orientation angles but ignore slight changes in the internal structure of each interacting molecule. Unfortunately, the actual development of parameters or recipes for effective dispersion or repulsion forces for a wide variety of species is not now available for the two X−M sequences of interest here. Furthermore, the order of electrostatics that has been applied to van der Waals molecules extends to higher order polarizabilities that are unavailable for HO_2. However, important electrostatic and dispersion information can be assembled for HO_2 and all of the M species. Concerning the electrostatics, the dipole moment vector μ of H_2O and the quadrupole moment Q of H_2O, H_2, N_2, and O_2 are all available.[41,50,57,58] The different diagonal components of the polarizability, α_{ii}, of all the M species in this study are known.[50,52,59,60] The average polarizabilities, $\langle\alpha\rangle$, of HO_2 have been estimated by Paul.[41] For the H_2O case, the entire polarizability tensor is known. While Paul also tabulated the dipole moment of HO_2, we have carried out relatively high-level electronic structure calculations[61] to obtain both the dipole moment vector and quadrupole moment tensor **Q**. These values and the electrostatic information for all the M species are assembled for convenience in Table 3. They allow the construction of the electrostatic component of the potential up through the quadrupole order.

The dispersion component at long range goes as the inverse of the center of mass distance to the sixth power, i.e., R^{-6}. The corresponding C_6 can be approximately evaluated through the standard[30] formula:

$$C_6 = \langle\alpha_1\rangle\langle\alpha_2\rangle I_1 I_2/(I_1 + I_2) \qquad (9)$$

which requires the polarizabilities in Table 3 and the ionization potentials, I, for species 1 and 2. The I values for HO_2 and all the species of M have been tabulated[41,59] and are listed in Table 3. This dispersion formula is specific to the interaction of

TABLE 3: Parameters for the Construction of Electrostatic and Dispersion Interaction Potentials

properties	He	Ne	Ar	Kr	H_2	O_2	N_2	CH_4	H_2O	HO_2
					Dipole Moment[a] (*D*)					
μ_x									0.0	1.61
μ_z									1.87	1.38
μ									1.87	2.12
					Quadrupole Moment[b] (au)					
Q_{xx}					−0.237	−0.125	0.56		1.96	0.595
Q_{yy}					−0.237	−0.125	0.56		−1.86	−0.469
Q_{zz}					0.474	0.250	−1.12		−0.10	−0.127
Q_{xz}					0.0	0.0	0.0		0.0	1.902
					Dipole Polarizability[c] (Å^3)					
α_{xx}	0.205	0.396	1.641	2.484	0.703	1.213	1.537	2.593	1.528	1.95
α_{yy}	0.205	0.396	1.641	2.484	0.703	1.213	1.537	2.593	1.415	1.95
α_{zz}	0.205	0.396	1.641	2.484	1.013	2.313	2.237	2.593	1.468	1.95
α	0.205	0.396	1.641	2.484	0.8066	1.580	1.770	2.593	1.470	1.95
					Ionization Potential[d] (eV)					
	24.587	21.564	15.759	13.999	15.427	12.063	15.576	12.6	12.6	11.53

[a] For H_2O, ref 41; for HO_2, ref 61. [b] Here $Q_{ab} = 3\sum q_i a_i b_i - \delta_{ab}\sum q_i r_i^2$ where q_i is the charge and δ_{ab} is the delta function. For H_2 and H_2O (with a geometry in the *xz* plane aligned along *z* axis), ref 50; for O_2, ref 57; for N_2, ref 58; for HO_2, ref 61 with a geometry in the *xz* plane of H(0.864,0.923), O(−0.066,0.640), and O(0.011,−0.698) in Å. [c] For rare gases and CH_4, ref 59; for H_2 and H_2O, ref 50; for O_2, ref 60; for N_2, ref 52; for HO_2, ref 41. [d] For all species except HO_2, ref 59; for HO_2, ref 41.

spherical atoms or molecules but, in the absence of any other convenient estimation, will still be applied here to any X−M interaction.

With the results in Table 3, an approximation to all but the short-range repulsive part of interaction potential can be constructed for X−M. Because of the absence of the short-range part, such an interaction potential cannot provide an independent value of r_e. But at the van der Waals value of r_e, the minimum value of the angularly dependent potential can be evaluated and compared to the van der Waals value of ϵ. That resulting minimum value is plotted with the van der Waals ϵ in Figure 7c with a greatly expanded ordinate scale. As expected, the electrostatic potentials produce more consistent energetics relative to the van der Waals information. There are some trends that are less ideal, in particular, the overestimation of the HO_2−H_2O interaction and the growing deviation in the diatomic−polyatomic sequence between the electrostatic minimum energy and the van der Waals ϵ with the mass of the rare gas. This is probably due to the lower order polarizabilities that are used. Also, there has been no attempt to check the angular coordinates at the electrostatic minimum energy with the same coordinates at the van der Waals minimum. In the future, there may be a role for a direct incorporation of "serious" van der Waals potentials in the study of collision rate constants for the low-pressure limit of recombination. However, the sole scope of this study is simply to qualitatively see if such potentials can have an important effect.

The electrostatic potentials can have both attractive and repulsive regions, making comparisons between the HO_2−M and H_2O−M sequences complicated. Nonetheless, the attractive regions of interaction potentials of the HO_2−M sequence have overall more negative potential energies than comparable regions of the interaction potentials of the H_2O−M sequence at the same value of *R*. Just the opposite is the case for the BP interaction potentials. Furthermore, attractive regions of electrostatic potentials tend to be more attractive at the same *R* than the BP potentials in a way that scales, in a qualitative sense, with the strength of the permanent moments. As mentioned before, BP potentials are effective potentials that do not need to reproduce actual potentials. However, to be meaningful, BP potentials must be some sort of average of the actual potentials. From the above considerations, the qualitative differences between electrostatic and BP potentials suggest that either the BP potentials are imperfect or this averaging happens to systematically suppress the effect of permanent moments in the interaction and systematically washes out the strength of the HO_2 interaction relative to that of H_2O.

C.2. Collision Rates from Collision Integrals. Given the new electrostatic interaction potentials, one could attempt to determine $\Omega^{22}\bigstar$, leading to an evaluation of Z_{coll} with eq 8. However, since the electrostatic potentials are not spherically symmetric, the usual formulation of $\Omega^{22}\bigstar$ would have to be generalized to account for rotationally inelastic collisions, and classical trajectory calculations for each X−M pair would then have to be carried out. In the future this would be interesting to pursue, but our immediate goal is to ascertain whether electrostatic potentials have any important effect on Z_{coll}. Consequently, the electrostatic potentials have been spherically symmetrized by a straightforward angular average over all angles for a given *R*. This gives an even weight to attractive and repulsive regions. The resulting spherically symmetrized potentials produce values of $\Omega^{22}\bigstar$ which can then be used with eq 8 to determine values of Z_{coll}. However, because the short-range repulsive interactions have not been included in the potential, the potential has no minimum, and hence, there no value of either σ or ϵ (used in the reduced temperature T^* at which $\Omega^{22}\bigstar$ is evaluated), both of which are required in the eq 8 formula for Z_{coll}.

Short of doing electronic structure calculations to directly obtain the potential energy surface, there is no independent information available to allow an estimation of the repulsive interactions of HO_2−M. Nonetheless, there are ways to estimate r_e and hence σ through the approximate Lennard-Jones relationship of $\sigma = 2^{1/6} r_e$. For HO_2−H_2O, the already cited calculations give r_e. This value of r_e is considerably smaller than the analogous value for H_2O−H_2O because, as previously discussed, two hydrogen bonds, instead of one, can be formed in HO_2−H_2O. That difference will not occur for any other of the M species, and the value of r_e for these M species interacting with HO_2 should be similar to the values of r_e already cited for these species interacting with H_2O. Once r_e is available, ϵ can be approximated by the value at r_e of the electrostatic and dispersion potential itself, as was indicated in Figure 7. The resulting r_e (or σ) and ϵ values complete the information needed for eq 8 use.

The final values of Z_{coll} as a function of temperature are displayed in panel b of Figure 6 for the same species of M as

used in panel a.[62] Relative to panel a of the same figure, using much stronger interaction potentials based on electrostatics has tended to make all Z_{coll} values only slightly different from the BP method; i.e., there is no qualitative change and, if anything, Z_{coll} is smaller. The clustering of Z_{coll} as a function of M, including H_2O, still persists. It is at first surprising that the Z_{coll} for HO_2-H_2O is not substantially larger, even though the interaction potential has qualitatively changed. This lack of change is due to a cancellation of effects specific to eq 8. The much deeper electrostatic potential does produce a considerably larger $\Omega^{22}\bigstar$, but the effect on Z_{coll} is canceled out by the smaller value of σ^2 because the much deeper potential occurs at smaller separations of HO_2 from H_2O. The absence of short-range interactions in the potentials does affect the calculated values of $\Omega^{22}\bigstar$. However, the effect is most likely minor. For example, consider an attractive $-C_6/r^6$ potential whose C_6 value is adjusted to give $-\epsilon$ in energy at $r_e = 2^{1/6}\sigma$ for some given (σ, ϵ) values. This purely attractive potential exactly matches at r_e the well depth of the Lennard-Jones potential for the same (σ, ϵ) values. At the same value of $T^* = kT/\epsilon$, the resulting $\Omega^{22}\bigstar$ value for the C_6 potential will exceed by only 5% − 25% the Lennard-Jones value over the entire range of (σ, ϵ) values found in Table 2. This change is in the wrong direction and at too small a scale to influence the analysis of the recombination kinetics.

The lack of a qualitative change between panels a and b in Figure 6 indicates that more realistic potentials are not in themselves sufficient to rationalize the observed recombination kinetics. This conclusion strongly suggests that the identification of $\pi\sigma^2\Omega^{22}\bigstar$ as the cross section appropriate for the collision rate, is incorrect for at least the interaction of HO_2* with polar colliders such as H_2O. Note that the identification of $\pi\sigma^2\Omega^{22}\bigstar$ with the collision cross section is not derivable from first principles. Rather it is observational and stems originally from studies done in the early 1950s. While eq 8 has been used successfully for decades, the experimental results of Table 1 call into question its applicability to at least the $H + O_2 + H_2O$ reaction.

C.3. Collision Rates without Collision Integrals. The term "collision rate" is not precise. Not all collisions (e.g., elastic collisions) are relevant to the low pressure limiting recombination process. There have been at least two different attempts to determine collision rates in the context of inelastic processes that are relevant to recombination kinetics. One of these attempts has been developed from of the study of inelastic collisions where one partner has only a modest amount of internal excitation, generally far less than chemically activated collision complexes that are at issue in recombination kinetics. Nonetheless, this development will be discussed first since it sets the stage for the second approach that is grounded in observations from classical trajectory studies of collisional relaxation of chemically activated species.

It has frequently been assumed that an initially excited molecule can be most efficiently collisionally de-excited if it can form a collision complex.[63] In some cases, the collision complex has been assumed to be so dominant in collisional de-excitation that the thermal rate of deactivation and the thermal rate of complex formation have been presumed to be essentially identical.[63] In the OH + CO recombination case, trajectory studies[64] confirm that de-excitation of CO(v=1) is entirely dominated by trajectories that form the HOCO complex even though most trajectories are direct repulsive encounters that never form this complex. This means that the high-pressure limit of recombination is a good measure of the rate of de-excitation of one of the reactants undergoing recombination.

The identification of a de-excitation rate with a complex formation rate has only been made in the case of a few quanta of excitation in one of the reactants. This is not the same as a chemically activated species (such as HO_2*) under consideration here. Nonetheless, accepting this identification suggests that one could use the interaction potential for HO_2-M to compute a complex formation rate and equate that rate to Z_{coll}. Since potentials under consideration for HO_2 + M have barrierless minimum energy paths (MEP) converging onto their most attractive regions, variational flexible transition state theory[65] (FTST) should be appropriate for computing the complex formation rate. FTST divides the internal degrees of freedom of the collision into conserved vibrational degrees of freedom (present in both reactants and the complex), transitional degrees of freedom (vibrational modes in the complex but free rotor modes in the reactants), and a degree of freedom for measuring progress along the MEP that becomes a vibrational mode in the complex.

The simplest form[66] of FTST is the canonical form where the conserved vibrational frequencies and reactant moments of inertia are assumed not to change along the reaction path and where the optimal reaction path coordinate is assumed to be R, the separation of the centers of mass of the reactants. In this simple form, FTST focuses only on the complex formation effects both of $V_{MEP}(R)$ (the potential along the MEP) and of steric hindrance created by hindered rotations that are evolving from the transitional modes with progress along the MEP. In this form, the FTST for the collision rate can be formulated[66] in a manner similar in appearance to eq 8:

$$Z_{coll}^{FTST-HR} = \langle v \rangle \pi\sigma^2 \min\{(R/\sigma)^2 e^{-V_{MEP}(R)/kT}\Gamma(R,T)\} \quad (10)$$

where

$$\Gamma(R,T) = \int e^{-\Delta V(\mathbf{q},R)/kT}\, d\mathbf{q} / \int d\mathbf{q} \quad (11)$$

The minimization is with respect to R where (a) the $\mathbf{q}$ values are specific orientational degrees of freedom describing hindered rotations away from the MEP, (b) $\Delta V(\mathbf{q};R)$ is the change in the interaction potential from $V_{MEP}(R)$ due to motion in $\mathbf{q}$, and (c) the Z_{coll} superscript, FTST-HR, emphasizes the inclusion of hindered rotations. $\Gamma(R,T)$ is a normalized steric hindrance factor that is unity in the case of a free rotor but is a fraction otherwise. The minimization process in eq 10 is applied to an expression that grows large at large R because of the R^2 factor (which comes from the moment of inertia for external rotations) and also grows large at small R because of the exponential factor for the attractive $V_{MEP}(R)$ potential. The minimum is found at some intermediate R between these two extremes. The minimized expression in eq 10 replaces $\Omega^{22}\bigstar$ in eq 8; however, there is no known formal derivation that connects the two.

Given eqs 10 and 11 and the electrostatic potentials discussed above, $Z_{coll}^{FTST-HR}$ can be computed for each M in the HO_2-M sequence by using the freeware code VARIFLEX.[67] The resulting values as a function of temperature are plotted in panel c of Figure 6. Comparison between panels b and c shows results that are qualitatively similar, indicating that there is not a substantial difference between eqs 8 and 10 for estimating collision rate constants. (Furthermore since no short-range repulsive terms have been added to the potential, the complex formation rate constant and hence Z_{coll} in panel c are, if any thing, overestimated.) Panels a−c still show a collision rate for $HO_2 + H_2O$ that is similar to the rates of other HO_2 + M, even

though the recombination rate of $H + O_2$ is 10 times larger in H_2O than in other M species. Thus, the requirement of unrealistic or unphysical values of $-\Delta E_{all}$ to rationalize the $H + O_2 + H_2O$ measurements persists.

While the origin of eq 10 lies in experimental and theoretical studies of initial excitations of only a few quanta, there are at least two relevant series of exclusively theoretical trajectory studies on the collision rate constants for chemically activated species. Lendvay and Schatz[68,69] studied energy transfer between CS_2* and most of the same collision partners under investigation here. Brown and Miller[70] studied HO_2* + He in the first detailed trajectory study of energy transfer ever done for the conditions of chemical activation. The motivation for these studies was to understand how chemical activation influences energy transfer and, for Lendvay and Schatz, to extensively compare theoretical estimates of ΔE_{all} with direct experimental measurements. However, as both sets of authors point out, direct measurements in fact measure the product, $Z_{coll}\Delta E_{all}$. All experimental studies assume a value for Z_{coll} (typically determined from eq 8 by selecting effective Lennard-Jones parameters) and then use that value to reduce the directly measured product to a measured ΔE_{all}.

All trajectory studies of energy transfer must resolve the problem posed by the infinite extent of the elastic cross section in classical mechanics. (The actual finite size of elastic cross sections arises out of quantum interference effects.) With unbounded elastic cross sections, the way to properly average very small transfers of energy at very large collision impact parameters becomes problematic. Lendvay and Schatz solved this problem by imitating experiment and directly calculating not ΔE_{all} but rather $Z_{coll}\Delta E_{all}$.

Direct trajectory calculation of the product implies the evaluation of the integral

$$\int_0^\infty \Delta E_{all}(b) b \, db \tag{12}$$

where $\Delta E_{all}(b)$ is the average energy transfer of all trajectories that started with impact parameter, b. With enough calculated classical trajectories, this integral properly converges. The maximum impact parameter, b_{max}, needed to converge the integral to some given convergence tolerance then defines the collision rate as

$$Z_{coll}^{traj} = \langle v \rangle \pi b_{max}^2 \tag{13}$$

Brown and Miller used a less rigorous approach. They selected a $b_{max,0}$ beyond which energy transfer was very small, binned their trajectories according to the amount of final energy transfer they displayed, fit an assumed functional form to part of the resulting distribution, and derived from the function, ΔE_{all}. In deriving the fit, they omitted the bin for the smallest energy transfers (which typically constituted ~40% of the trajectories run). Extrapolating the fit down to zero energy transfer leads to a way to derive only the inelastic component of the nominal calculated total (elastic and inelastic) cross section of $\pi b_{max,0}^2$. From the inelastic cross section, the effective b_{max} can be determined. Because the results are subject to imperfections in a fit, the derived inelastic cross sections and consequent Z_{coll} are less secure than those of Lendvay and Schatz. In what follows, the implications of the Lendvay and Schatz studies will first be discussed followed by a review of the Brown and Miller study.

If eqs 8 and 13 are compared, then $b_{max} = \sigma(\Omega^{22}\bigstar)^{1/2}$. Lendvay and Schatz then compared[68] b_{max} values (using the

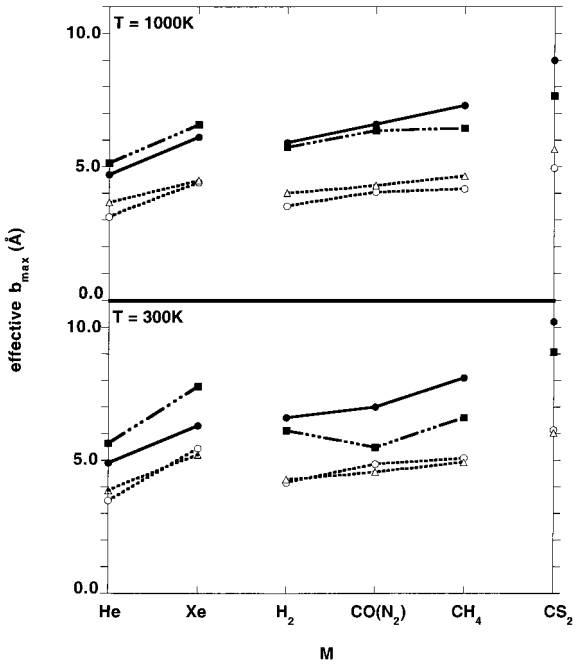

Figure 8. Effective b_{max} versus bath gas species M for the CS_2* + M sequence as determined by trajectories (●), by $\Omega^{22}\bigstar$ determined from experimental Lennard-Jones parameters (△), by $\Omega^{22}\bigstar$ determined from the potential energy surface (○), and by a free rotor model (■). See text for details.

Lennard-Jones parameters from an experimental study) with trajectories calculations for two sequences: CS_2* + M (=He, Ar, Xe, H_2, N_2, CH_4 and CS_2) and SF_6* + M (=Ar and SF_6). The potential energy surfaces used for the trajectories were pairwise additive Lennard-Jones potentials constructed from tabulated[71] rare gas Lennard-Jones parameters under the assumption that the interaction between atoms A and B would be the same as that for a rare gas in the same row of the periodic table as A, interacting with a rare gas in the same row as B. Lendvay and Schatz had already shown that such potentials were reliable in comparing theory to experiment.[69] While CS_2* and SF_6* were first given a large amount of initial energy (93 kcal mol^{-1}), the third-body M had thermal distributions characterized by 300 K, 1000 K, and in some cases, 1500 K. The conclusion from the study was that eq 8 systematically underestmates Z_{coll} by typically a factor of 2. This study suggests that the success of eq 8 in estimating Z_{coll}, over several decades of recombination and inelastic studies, is *not* due to its intrinsic accuracy but rather to the fact that it is well matched to selected $-\Delta E_{all}$ values. They pointed out that noticeably higher Z_{coll} values, and correspondingly lower $-\Delta E_{all}$ values, could equally well match the available experimental data.

While the Lendvay−Schatz study did not include any polar−polar interactions (which would be most relevant here), the CS_2* + M sequence does involve a chemically activated triatomic molecule with many of the same M species under consideration here. One possible difficulty with the Lendvay−Schatz study on CS_2* + M is that the comparison with $\sigma(\Omega^{22}\bigstar)^{1/2}$ used experimental estimates of the effective Lennard-Jones parameters rather than spherically symmetrized interaction potentials directly derived from the potential energy surfaces that were used in the trajectory studies. In Figure 8, we reproduce the Lendvay−Schatz results for CS_2* + M for the same M species used here with HO_2, and we also include the values of $\sigma(\Omega^{22}\bigstar)^{1/2}$ that arise from spherically symmetrizing the potential energy surfaces used in the trajectory calculations. The two panels in the figure are specific to bath gas temperatures of 300

and 1000 K. The figure shows no qualitative difference between the experimentally selected effective Lennard-Jones parameters or those derivable from the potential energy surfaces used in the trajectory calculations. The b_{max} determined by the trajectories is systematically larger than either estimate of $\sigma(\Omega^{22}\bigstar)^{1/2}$, leading to Z_{coll}^{traj} values ~1.5−2.0 times larger than those from eq 8.

These results would suggest that a trajectory study to converge the integral of eq 12, using the electrostatic potentials for the HO_2^* + M sequence, could produce Z_{coll} and $-\Delta E_{all}$ values that are both internally consistent and physically meaningful. However, such a study is beyond the scope of this paper and will not be reported on at this time. Instead, a simple heuristic approach will now be developed to qualitatively reproduce the results of Lendvay and Schatz. This approach can then be readily applied to the HO_2^* + M sequence to estimate what a rigorous trajectory study would likely produce for Z_{coll}^{traj}.

The heuristic approach starts from the $Z_{coll}^{FTST-HR}$ calculations discussed previously. The effect of incorporating hindered rotations, through the steric factor, $\Gamma(R,T)$, is to strongly weight the most attractive parts to the potential energy surface, especially at lower temperatures; i.e., those parts that are closest in energy to $V_{MEP}(R)$ where ΔV in eq 11 in near to zero. While this might be appropriate when one of the reactants has only a few quanta of excitation, as the amount of excitation increases, one might expect that even the repulsive parts of the potential energy surface would be effective in forcing some de-excitation. As the degree of excitation increases, the fractional $\Gamma(R,T)$ factor would then become an increasingly overly restrictive limitation on the size of Z_{coll}. In the limit of high initial excitation, one might expect that all parts of the interactive potential, whether strongly attractive or strongly repulsive, should induce de-excitation. In this limit, the Boltzmann factor in $\Gamma(R,T)$ that favors only the attractive portions of the potential energy surface should be removed. This is equivalent to setting $\Gamma(R,T)$ to its maximum possible value of unity and reduces the calculation of a collision rate to one that effectively involves free rotors for all the orientational degrees of freedom. The resulting expression for the collision rate from eq 10 then becomes

$$Z_{coll}^{FTST-FR} = \langle v \rangle \pi \sigma^2 \min\{(R/\sigma)^2 e^{-V_{MEP}(R)/kT}\} \qquad (14)$$

where the Z_{coll} superscript emphasizes the free rotor assumption. In this formulation, the effective b_{max} would be min$\{Re^{-V_{MEP}(R)/2kT}\}$. (In the case of marginally attractive $V_{MEP}(R)$, the {} factor in eq 14 does not have a minimum. Then, the closest approximation to a minimum, namely the minimum in the derivative of the {} factor, is used.)

Under the assumption that the limiting case of high initial excitation applies to the Lendvay−Schatz studies, eq 14 has been applied using a $V_{MEP}(R)$ determined as the mininum value at each value of R of the potential energy surface used for the trajectories for each CS_2^* + M combination. The result of the minimization procedure for most CS_2^* + M combinations shows multiple minima whose positions vary with temperature. If the minimum at the largest value of R (which is often *not* the deepest minimum) is selected in the evaluation of eq 14, the resulting values of the min$\{Re^{-V_{MEP}(R)/2kT}\}$ are those displayed in Figure 8. While not in perfect agreement with the trajectory values of b_{max}, these values are of comparable size and show the same trends with changes in M. Though imperfect, eq 14 offers an inexpensive way to approximate Z_{coll}^{traj} with $Z_{coll}^{FTST-FR}$.

As mentioned above, the Brown and Miller trajectory study[70] on HO_2^* + He also determined Z_{coll}^{traj}. The potential energy surfaces used for the trajectories were similar in spirit to that of Lendvay and Schatz but with Lennard-Jones potentials replaced by more complicated potentials derived from molecular beam studies of He−He and He−Ne. While HO_2^* was given an initial energy (46 kcal mol^{-1}) right at the threshold of dissociation on their potential energy surface, the He had thermal distributions characterized by 800, 2000, and 5000 K. Unlike Lendvay and Schatz, a variety of initial rotational distributions were examined, producing a distribution of Z_{coll}^{traj} values with a ~15% spread about the mean. Using standard Lennard-Jones parameters to evaluate eq 8, Brown and Miller concluded that Z_{coll}^{traj} were ~30% larger at 800 K than that determined from eq 8. (Lendvay and Schatz get ~225% larger for CS_2^* + He at 1000 K.) With the same potential energy surface used by Brown and Miller, $Z_{coll}^{FTST-FR}$ can be calculated. To compare this calculation in a spirit similar to Figure 8, the effective b_{max} for Brown and Miller is 3.42 ± 0.23 Å at 800 K, while that for $Z_{coll}^{FTST-FR}$ is 4.12 Å. As in Figure 8 for M = He, the FTST-FR approximation overestimates the effective b_{max}, but by 21 ± 8% for HO_2^* at 800 K as opposed to 9% for CS_2^* at 1000 K. Given the uncertainty discussed above in the Brown and Miller derivation of the inelastic cross section from trajectories, the Z_{coll}^{traj} from both the Brown and Miller and the Lendvay and Schatz studies are imperfectly, but reasonably, represented by $Z_{coll}^{FTST-FR}$.

In this spirit, eq 14 can be applied to the HO_2^* + M sequence. The application is more straightforward than in the CS_2^* + M sequence because it so happens that for every M at every temperature, there is only one minimum. The resulting values of $Z_{coll}^{FTST-FR}$ are displayed in panel d of Figure 6. In general, the collision rate constants in panel d are higher than their counterparts in any other panels. However, the differences become largest for those species with permanent moments (H_2, O_2, N_2, and H_2O). This causes the spread of Z_{coll} values as a function of M to be larger than in any other panel. Furthermore, for H_2O, the collision rate is more than 2 times larger than the analogous values in the other panels and is now much larger than that for almost all other M species.

D. Final Experiment to Theory Comparison. With the results in panel d, the experimental recombination results can be theoretically reanalyzed. The same theoretical approach used above with the BP method (panel a in Figure 6) is repeated with the new panel d estimates; i.e., $Z_{coll}^{FTST-FR}$. The strong collision low-pressure limiting rate constants are evaluated with eq 5. As before, with insertion of the low-pressure limits, along with the high-pressure limits, into the complete Troe theory,[4−7] the rate constants can be predicted at any temperature or pressure and can be compared to experiments with $-\Delta E_{all}$ being the adjustable parameter. The final results are represented as the solid lines in Figures 9−13 for M = O_2, N_2, H_2, He, and Ar. The resulting values of $-\Delta E_{all}$ are listed in Table 4. Table 4 also lists room-temperature results for M = He, Ne, Ar, Kr, H_2, N_2, O_2, and CH_4.

Figure 9 shows a summary of the present data for O_2 (i.e., eq 3 as the bold dashed line) along with a theoretical prediction using $-\Delta E_{all}$ = 95 cal mol^{-1} (33.2 cm^{-1}) for the experimental pressure of ~90 Torr. This $-\Delta E_{all}$ gives values for β_c of 0.150−0.024 between 200 and 1500 K. Even though most workers have assumed that the relative efficiency of O_2 to N_2 is unity,[72] we find that O_2 is less efficient, being between N_2 and the rare gases. There are no earlier direct values for comparison. With N_2, Figure 10 shows eq 2 in comparison to earlier direct[17−19] and derived[27,28,73−77] T-dependent rate constant determinations. Considering combined experimental errors, most of these determinations satisfactorily agree, with the exception of the

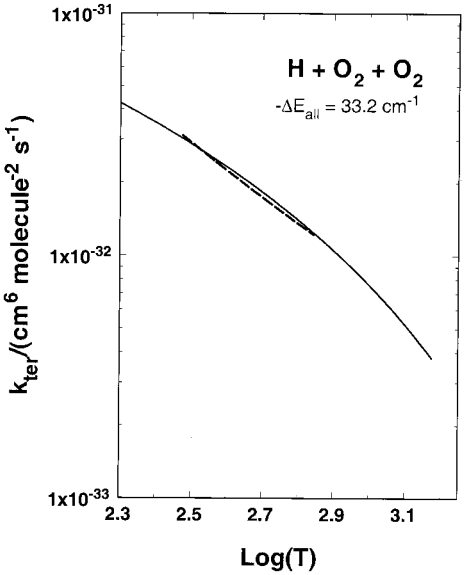

Figure 9. Comparison of the experimental (dashed line) and theoretical (solid line) k_{ter} for $H + O_2 + O_2$. The experimental rate expression is derived from the linear-least-squares fit of the present data summarized in Figure 5 and eq 4. The theoretical rate constants require $-\Delta E_{all} =$ 95.0 cal mol^{-1} at ~90 Torr.

TABLE 4: Optimized Values of $-\Delta E_{all}$ and β_c as a Function of Temperature for Different Bath Gases[a]

bath gas	T/K	$-\Delta E_{all}$/cm^{-1}	range of β_c	k_{ter}/(10^{-32} cm^6 molecule^{-2} s^{-1})
H_2O	300	210	0.38	48.2
CH_4	300	210	0.38	14.3
N_2	300	38.5	0.19	4.03
O_2	300	33.2	0.11	2.99
H_2	300	26.3	0.087	6.10
He	300	23.0	0.078	2.28
Ne	300	23.0	0.078	1.52
Ar	300	23.0	0.078	1.97
Kr	300	23.0	0.078	1.94
H_2O	200−1500	210	0.47−0.12	
N_2	200−1500	38.5	0.16−0.028	
O_2	200−1500	33.2	0.15−0.024	
H_2	200−1500	$8.39T^{0.2}$	0.11−0.026	
He	200−1500	$7.35T^{0.2}$	0.10−0.023	
Ar	200−1500	$7.35T^{0.2}$	0.10−0.023	

[a] For room temperature measurements, the calculated termolecular rate constant is also given.

higher temperature values of Carleton et al.[19] We also show three theoretical calculations at 15 Torr, 10 atm, and 50 atm, respectively, from top to bottom in the figure, obtained with $-\Delta E_{all} = 110$ cal mol^{-1} or 38.5 cm^{-1} ($0.160 \leq \beta_c \leq 0.023$, for 200−1800 K). With the exception of the present work, all previous work above ~650 K was carried out between 1 and 50 atm whereas all lower-T work was between 1 and ~500 Torr. We believe that some of the discrepancy noted in earlier work may have been partially due to a lack of appreciation of the slight pressure sensitivity shown by the theoretical calculations. There is minimal T-dependent data for H_2 bath gas,[18,26,78] but this is shown in Figure 11 along with a theoretical calculation at 500 Torr with a slightly T-dependent energy transfer parameter, $-\Delta E_{all} = 24.0T^{0.20}$ cal mol^{-1} K$^{-0.2}$ ($8.39T^{0.20}$ cm^{-1} K$^{-0.2}$), implying $0.110 \leq \beta_c \leq 0.026$, for 200−1500 K. For the available data, theory agrees satisfactorily with experiment.

T-dependent determinations with rare gases are more extensive than with di- or polyatomic molecules. The present 296 K and earlier results[17,18,24,25,73] at higher temperatures with He bath

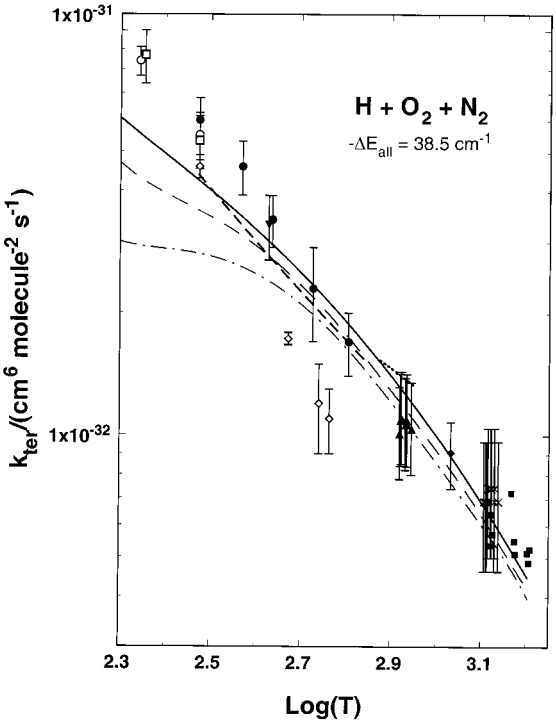

Figure 10. Comparison of the experimental and theoretical (solid lines) k_{ter} for $H + O_2 + N_2$. The experimental rates include direct measurements by (□) Kurylo at 40 Torr (ref 17), (○) Wong and Davis at ~30 Torr (ref 18), (◇) Carleton et al. at 350 Torr (ref 19), and (− − −) present work, eq 2. Derived experimental data include (■) Getzinger and Blair at 2.5 atm (ref 27), (×) Davidson et al. at ~50 atm (ref 28), (●) Hsu et al. at ~15 Torr (ref 73), (◆) Slack (ref 74), (▼) Campbell et al. at 1.5−3.5 Torr (ref 75), (▲) Mueller et al. at 10 atm (ref 76), and (- - -) Ashman et al. (ref 77). The three lines are theoretical calculations of rate constants using $-\Delta E_{all} = 110$ cal mol^{-1}, from top to bottom, at 15 Torr, 10 atm, and 50 atm, respectively.

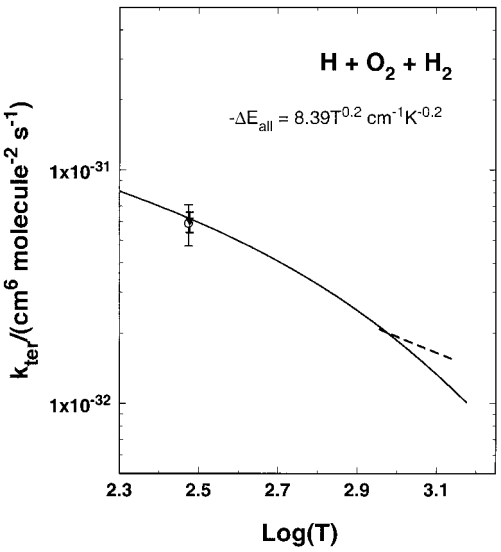

Figure 11. Comparison of the experimental and theoretical (solid line) k_{ter} for $H + O_2 + H_2$. Three experimental measurements are by (▼) Wong and Davis at 20 Torr (ref 18), (○) Nielsen et al. at 1 atm (ref 26), and (− − −) Kochubei and Moin at ~500 Torr (ref 78). The theoretical rate constant calculations require $-\Delta E_{all} = 24.0T^{0.2}$ cal mol^{-1} K$^{-0.2}$ at 500 Torr.

gas are shown in Figure 12. The data at room temperature are in moderate agreement, with the value of Kurylo[17] being the lowest. Certainly, if all data shown in Figure 12 are compared at the two standard deviation level, then the data agree; however, the values of Kurylo are probably still low even though this

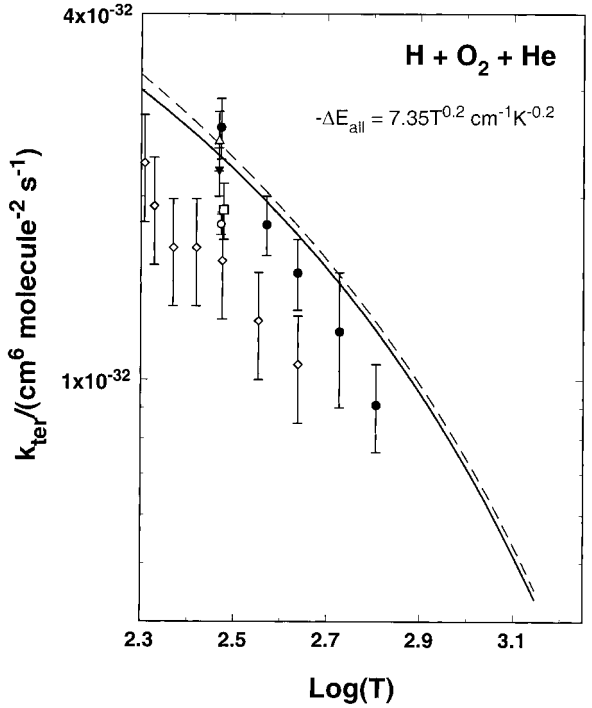

Figure 12. Comparison of experimental and theoretical k_{ter} for H + O_2 + He. Experimental direct measurements are by (○) present work, (◇) Kurylo at ~150 Torr (ref 17), (□) Wong and Davis at 50 Torr (ref 18), (△) Hack et al. at 3.75 Torr (ref 24), and (▼) Clyne and Thrush at ~3 Torr (ref 25). Derived experimental rates are from (●) Hsu et al. at 15 Torr (ref 73). The two theoretical lines are based on $-\Delta E_{all} = 21.0T^{0.2}$ cal mol^{-1} K$^{-0.2}$ at 3.8 Torr (dashed line) and 500 Torr (solid line), respectively.

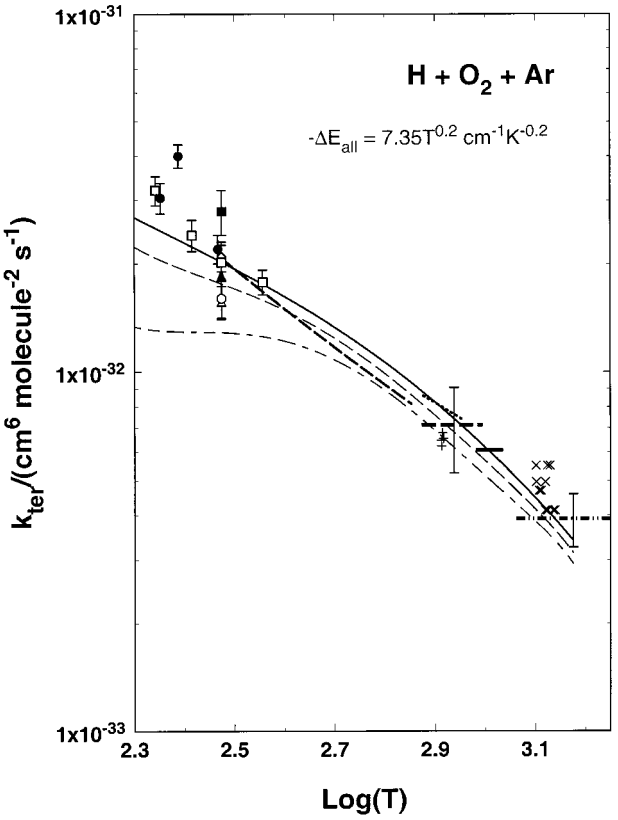

Figure 13. Comparison of experimental and theoretical k_{ter} for H + O_2 + Ar. The experimental rate constants include direct measurements by (△) Kurylo at 40 Torr (ref 17), (□) Wong and Davis at ~30 Torr (ref 18), (◇) Carleton et al. at 350 Torr (ref 19), and (○) Hidika et al. at ~1 atm (ref 22), and (− − −) present work. Derived experimental rates are from (■) Cobos et al. (ref 20), (▲) Westenberg and deHaas (ref 23), (●) Clyne and Thrush (ref 25), (×) Davidson et al. at ~50 atm (ref 28), (— —) Slack at 3 atm for 964−1075 K (ref 74), (+) Mueller et al. at 10 atm (ref 76), (- - -) Ashman et al. at 1 atm (ref 77), (—••—••—) Getzinger and Schott at 3.5 atm for 1150−1850 K (ref 79), and (—) Pirraglia et al. for 746−987 K (ref 80). The three theoretical lines are calculations using $-\Delta E_{all} = 21.0T^{0.2}$ cal mol^{-1} K$^{-0.2}$, from top to bottom, at pressures, 3 Torr, 10 atm, and 100 atm, respectively.

was a direct determination. We show two theoretical predictions with $-\Delta E_{all} = 21.0T^{0.20}$ cal mol^{-1} K$^{-0.2}$ or $7.35T^{0.20}$ cm^{-1} K$^{-0.2}$ (i.e., $0.110 \le \beta_c \le 0.023$, 200−1500 K) for pressures 3.8 (dashed line) and 350 Torr (solid line). These calculations are not sufficiently different to explain the spread of values at room temperature, but they do supply a compromise explanation that nearly reconciles all data except those of Kurylo. Rate constants in Ar bath gas are more extensive than those with He. The room temperature and T-dependent data[17−20,22,23,25,28,74,76,77,79,80] are plotted in Figure 13 and range in pressure from ~1−5 Torr[23,25] to 115 atm.[28] At room temperature, the data of Kurylo[17] and Hikida et al.[22] appear to be lower than the other studies. Because of the large range in pressure, three theoretical predictions at 3 Torr, 10 atm, and 100 atm with $-\Delta E_{all} = 21.0T^{0.20}$ cal mol^{-1} K$^{-0.2}$ or $7.35T^{0.20}$ cm^{-1} K$^{-0.2}$ (i.e., $0.110 \le \beta_c \le 0.019$, 200−1800 K) are shown in comparison to the data. The theory mostly reconciles all previous data and shows, as with N_2 bath gas, that pressure sensitivity has probably not been appreciated in earlier work.

Considering Figures 9−13, the level of agreement with the experimental data for these species of M is similar to that discussed in part B above with Z_{coll} evaluated in the standard way with eq 8 using the BP method. This includes the fact that, consistent with experiment, Z_{coll} is lowest for M = Ne in the rare gas series. This arises from contrasting trends, shared by eqs 8 and 14, of increasing cross section but decreasing average velocity as M goes from He to Xe. For all M except H_2O, the major effect of the new way of evaluating Z_{coll} is to decrease the optimized value of $-\Delta E_{all}$ so as to keep the product of $Z_{coll}\Delta E_{all}$ to be approximately the same.

The results for H_2O as the bath gas are displayed in Figure 14 and also listed in Table 4. The figure shows the present work along with other direct[19] and derived[25,29,73,77] values of k_{ter}. We have evaluated the pressure falloff using the methods given by Troe and co-workers[4−8] and display those results in the figure over the range of pressures sampled in the experimental record. The level of agreement between theory and experiment is comparable to that found in Figures 9−13 for other species of M. As indicated in Table 4, the theoretical prediction at room temperature and low pressure (15 Torr) requires a $-\Delta E_{all}$ = 600 cal mol^{-1} (210 cm^{-1}). Over an extended temperature range that encompasses the experimental record, β_c factors range from 0.47 to 0.12 between 200 and 1500 K. Such physically meaningful values of β_c can only be obtained with the large collision rates for M = H_2O indicated by $Z_{coll}^{FTST-FR}$ and displayed in panel d of Figure 6.

The $-\Delta E_{all}$ values that are reported in Table 4 have two interesting features. First, for all rare gas bath gases, $-\Delta E_{all}$ values are the same. For diatomic and polyatomic species of M, $-\Delta E_{all}$ values are larger and generally increase with the size or complexity of the molecules. We note that there are ~10 times more states in HO_2* at threshold than counted by considering vibrations alone. This is near to an energy continuum in which case there are a large number of rovibrational energy combinations available for transfer provided the acceptor molecule has a resonance available to accept the energy. Since

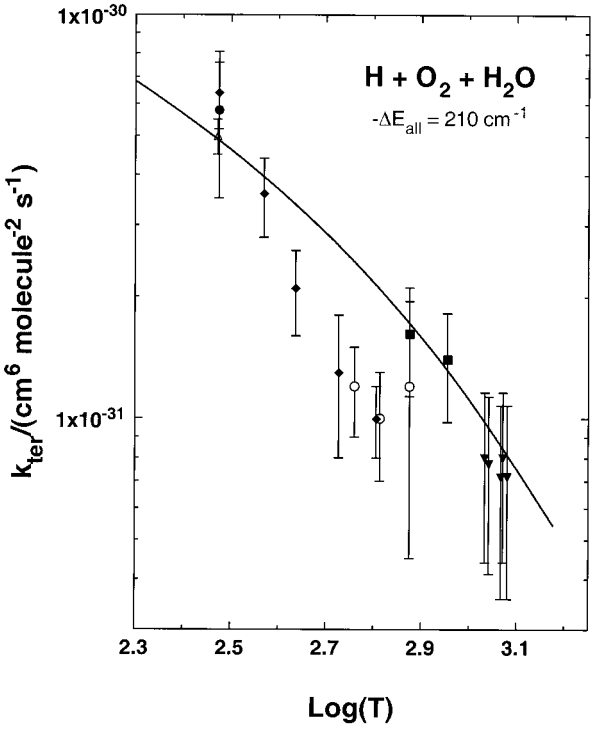

Figure 14. Comparison of experimental and theoretical k_{ter} for $H + O_2 + H_2O$. The direct measurement and derived experimental rate constants are open and solid symbols, respectively, each with its own error bar: (○) Carleton et al. (ref 19), (△) present work, (●) Clyne and Thrush (ref 25), (▼) Bates et al. (ref 29), (◆) Hsu et al. (ref 73), and (■) Ashman et al. (ref 77). The solid line is a theoretical rate constant calculation at 15 Torr with $-\Delta E_{all} = 600$ cal mol^{-1}.

the fundamental vibrational energies for the di- and polyatomic acceptor molecules considered here are substantially larger than the transferred energies, we suggest that energy transfer might essentially only be into translational and rotational degrees of freedom. Then one expects translational energy transfer to be similar to monatomics with the enhancement for di- and polyatomics to be predominantly due to rotations in the acceptors. H_2 appears to be an exception; however, we note that the rotational spacing in this molecule is sparse. Between $J = 0$ and 1 the energy difference is 121.6 cm^{-1} (i.e., 350 cal mol^{-1}). It therefore may be that the paucity of available states in H_2 decreases the probability for rotational energy transfer from the near continuum of states in HO_2* and that energy transfer to translations, as in monatomics, will be the more effective process with H_2. This would be reflected in the above derived $-\Delta E_{all}$ values for monatomics versus H_2 of $7.35T^{0.2}$ and $8.39T^{0.2}$ cm^{-1} K$^{-0.2}$, respectively.

As shown in Table 4, N_2 requires no temperature dependence while Ar has $-\Delta E_{all}$ increase by the temperature to the 0.2 power. This contrasts with the conclusions of Troe[8] who reports T-dependence in $-\Delta E_{all}$ for both N_2 and Ar. However, the final β_c values for both Ar and N_2 in Troe's report are almost identical to those found here because $-\Delta E_{all}$, in the present and previous work,[8] is adjusted in order to recover β_c's that reproduce essentially the same experimental data. The difference between our results and those of Troe lies in the treatment of Z_{coll} and the density of states of HO_2*. The difference in $-\Delta E_{all}$ values points out that this parameter is not independently obtained from kinetic data but instead is correlated with approximations or assumptions about other aspects of the rate constant, which also cannot be independently determined from kinetic data. This is essentially the conclusion of Lendvay and Schatz, discussed above, that $-\Delta E_{all}$ and Z_{coll} have never been independently measured.

Summary and Conclusions

The third-order reaction, $H + O_2 + M \rightarrow HO_2 + M$, has been measured near the low-pressure limit at room temperature for M = He, Ne, Ar, Kr, O_2, N_2, and H_2O and over an extended range of temperatures for M = Ar, O_2, and N_2. In all cases, H-atoms were produced by the laser photolysis of NH_3 and detected by atomic resonance absorption spectroscopy. All measurements were conducted in a shock tube, but the room temperature measurements used the shock tube as only a static pressure chamber. These measurements are the first reported for M = O_2. For the other M and also for H_2 and CH_4, previous measurements are available. All of these results are reviewed and compared. The measurements here are consistent with the available experimental record and, in particular, confirm the exceptionally high recombination rate constant when M = H_2O.

The standard theoretical analysis as first developed by Troe[4−7] is applied to this entire experimental record. The values of the average energy change per collision, $-\Delta E_{all}$, derived from that analysis, are sensible for all M but H_2O where the derived probability of stabilization has an unphysical value greater than unity at room temperature. This result motivated changes in the standard theoretical analysis that both rationalized the behavior of H_2O and also quantitatively reduced the derived $-\Delta E_{all}$ for other species of M:

- The number of active rotational degrees of freedom contributing to the HO_2* state density are made explicitly temperature dependent. In standard theory, pre-assigned values of which rotations are active or adiabatic are typically incorporated for all temperatures without any detailed justification.
- The Lennard-Jones potential for the HO_2* + M interaction is replaced with an electrostatic + dispersion potential. Such potentials are required to reliably represent interactions between polar−polar species. In contrast, the effective Lennard-Jones potentials typically applied in the standard analysis have never been validated by data reflecting polar−polar interactions.
- The collision rate between HO_2* + M on the electrostatic + dispersion potential is estimated by a free rotor model for "complex formation" between the bath gas and HO_2*. This approach can be physically motivated but is primarily justified by the ability of the method to reproduce trajectory collision rates by Lendvay and Schatz[68,69] and Brown and Miller[70] on related chemically activated systems. In contrast, the standard collision rate (a hard-sphere estimation modified by the collision integral $\Omega^{22}\star$) underestimates the trajectory collision rates, often by a factor of 2.

The optimized values of $-\Delta E_{all}$ that are produced from this new analysis have the following characteristics:

- Within experimental error, all rare gases have the same $-\Delta E_{all}$. For He and Ar, the only rare gas species for which temperature-dependent data exists, $-\Delta E_{all}$ increases slightly with temperature. The recombination rate constant is lowest for Ne because of contrasting trends in the energy transfer cross section and the average velocity of energy transfer collsions.
- There is clear enhancement in $-\Delta E_{all}$ for di- and polyatomic molecules relative to the rare gas atoms. In only one case (H_2) does the data justify a slight temperature dependence for $-\Delta E_{all}$.

Beyond the results specific to $H + O_2$ recombination, this work supports the importance of rotational contributions and their temperature dependence to the estimation of the density of states of activated complexes. Rotational contributions to the

state density of molecules at threshold have been reported in at least four cases, H_2CO,[81] C_2H_2,[82] and CH_3OH and but-1-yne.[83] The spectroscopically observed density of states at threshold is substantially larger than the vibrational state density even when anharmonically corrected, emphasizing the importance of rotations. A theoretical model that goes beyond the harmonic-oscillator/rigid-rotor formulas used here has not yet been developed to quantitatively explain the phenomena.

This work also strongly supports several lines of work that suggest that standard Lennard-Jones models underestimate collision rate constants. Most relevant to this study is the work of Lendvay and Schatz who concluded from classical trajectories that collision rates between activated complexes and bath gases may be *typically* underestimated by standard Lennard-Jones formulas. Since most experiments are much more sensitive to the product of the collision rate and $-\Delta E_{all}$ than to either individually, this is equivalent to claiming that $-\Delta E_{all}$ derived from recombination kinetics measurements are *typically* overestimated. Supporting experimental evidence that Lennard-Jones models underestimate collision rates comes from recent direct attempts to measure the total inelastic cross section for thermalized bath gas molecules striking target molecules with an initially fixed high internal energy. These experiments construct the cross section by directly measuring inelastic transition probabilities for the entire range of inelastic energy change. In a number of cases, the resulting cross-sections are larger than associated Lennard-Jones cross sections.[84] If the Lennard-Jones underestimation of the collision rate (or cross-section) is too severe, no derivation of $-\Delta E_{all}$ from recombination kinetics is possible because the probability per collision of stabilization exceeds unity. We believe this is precisely what happens in $H + O_2 + H_2O$ where strong polar−polar interactions makes the underestimation of the collision rate particularly severe.

This work strongly supports the original insight of Hsu et al.[21] who first pointed out the difficulty of rationalizing the large recombination rate constant of $H + O_2 + H_2O$. They recommended the equivalent of electrostatic potentials (although not as complete as those employed here) and a complicated approximate quantum mechanical calculation of the collision rate. Such quantum calculations are too elaborate for routine use and have approximations difficult to evaluate. Furthermore, the trajectory results of Lendvay and Schatz show that quantum effects are not necessarily an essential feature of the problem. Nonetheless, Hsu et al. pioneered the basic strategy that has been applied here.

Our work offers a method to evaluate the collision rate that can readily be put to routine use. Electrostatic moments of common bath gases are generally available and such moments can be estimated or calculated for activated complexes. The determination of a complex formation rate between the bath gas and the activated complex on an electrostatic + dispersion potential is quite straightforward with a free rotor model. However, while physically motivated at some level, the primary validation of this method lies in its ability to reproduce a few trajectory calculations. Clearly, more systematic and comprehensive comparisons of this approach with trajectory calculations will be required to develop confidence in the method.

Finally, if polar−polar interactions between M and HO_2* have a large enough effect to make the standard theoretical approach unphysical, then one might anticipate that the related standard theory for transport properties of polar−polar mixtures would be inadequate. The effective Lennard-Jones parameters used in recombination kinetics typically have their validation in their ability to reproduce measured transport properties. However, to our knowledge, there is no database of measured transport properties for polar−polar mixtures. If such measurements could be performed, both transport processes and recombination kinetics would benefit.

Acknowledgment. We thank L. Harding for electronic structure calculations on HO_2. We thank G. Schatz and G. Lendvay for helpful discussions. This work was supported by the U.S. Department of Energy, Office of Basic Energy Sciences, Division of Chemical Sciences, under Contract No. W-31-109-Eng-38.

References and Notes

(1) Westbrook, C. K.; Dryer, F. *Prog. Energy Combust. Sci*. **1984**, *10*, 1.

(2) DeMore, W. B.; Sander, S. P.; Golden, D. M.; Hampson, R. F.; Kurylo, M. J.; Howard, C. J.; Ravishankara, A. R.; Kolb, C. E.; Molina, M. J. *Chemical Kinetics and Photochemical Data for use in Stratospheric Modeling*; Evaluation No. 12; JPL Publication 97-4; JPL: Pasadena, CA, January 15, 1997.

(3) Mallard, W. G.; Westley, F.; Herron, J. T.; Hampson, R. F. *NIST Chemical Kinetics Database*, Version 6.0; NIST Standard Reference Data; NIST: Gaithersburg, MD, 1994.

(4) Troe, J. *J. Chem. Phys.* **1977**, *66*, 4745, 4758.

(5) Troe, J. *J. Phys. Chem.* **1979**, *83*, 114.

(6) Troe, J. *Ber. Bunsen-Ges. Phys. Chem.* **1983**, *87*, 161.

(7) Gilbert, R. G.; Luther, K.; Troe, J. *Ber. Bunsen-Ges. Phys. Chem.* **1983**, *87*, 169.

(8) Troe, J. *Proc. Combust. Inst.* **2000**, *28*, 1463.

(9) Michael, J. V. *J. Chem. Phys.* **1989**, *90*, 189.

(10) See Michael, J. V. In *Advances in Chemical Kinetics and Dynamics*; Barker, J. R., Ed.; JAI: Greenwich, CT, 1992; Vol I, p 47, for original references.

(11) Michael, J. V. *Prog. Energy Combust. Sci.* **1992**, *18*, 327.

(12) Michael, J. V.; Klemm, R. B.; Brobst, W. D.; Bosco, S. R.; Nava, D. F. *J. Phys. Chem.* **1985**, *89*, 3335.

(13) Maki, R. G.; Michael, J. V.; Sutherland, J. W. *J. Phys. Chem.* **1985**, *89*, 4815.

(14) Michael, J. V.; Lifshitz, A. In *Handbook of Shock Waves*; Ben-Dor, G., Igra, O., Elperin, T., Lifshitz, A., Eds.; Academic Press: New York, 2001; Vol. 3, pp 77−105.

(15) Michael, J. V.; Sutherland, J. W. *Int. J. Chem. Kinet.* **1986**, *18*, 409.

(16) Michael, J. V.; Fisher, J. R. *AIP Conference Proceedings 208, 17th Int. Symp. On Shock Waves and Shock Tubes* **1990**, *17*, 210.

(17) Kurylo, M. J. *J. Phys. Chem.* **1972**, *76*, 3518.

(18) Wong, W.; Davis, D. D. *Int. J. Chem. Kinet.* **1974**, *6*, 401.

(19) Carleton, K. L.; Kessler, W. J.; Marinelli, W. J. *J. Phys. Chem.* **1993**, *97*, 6412.

(20) Cobos, C. J.; Hippler, H.; Troe, J. *J. Phys. Chem.* **1985**, *89*, 342.

(21) Hsu, K.-J.; Durant, J. L.; Kaufman, F. *J. Phys. Chem.* **1987**, *91*, 1895.

(22) Hikida, T.; Eyre, J. A.; Dorfman, L. M. *J. Chem. Phys.* **1971**, *54*, 3422.

(23) Westenberg, A. A.; deHaas, N. *J. Phys. Chem.* **1972**, *76*, 1586.

(24) Hack, W.; Wagner, H. Gg.; Hoyermann, K. *Ber. Bunsen-Ges. Phys. Chem.* **1978**, *82*, 713.

(25) Clyne, M. A. A.; Thrush, B. A. *Proc. R. Soc. London, Ser. A* **1963**, *A275*, 559.

(26) Nielsen, O. J.; Sillesen, A.; Luther, K.; Troe, J. *J. Phys. Chem.* **1982**, *86*, 2929.

(27) Getzinger, R. W.; Blair, L. S. *Combust. Flame* **1969**, *13*, 271.

(28) Davidson, D. F.; Petersen, E. L.; Röhrig, M.; Hanson, R. K.; Bowman, C. T. *Proc. Combust. Inst.* **1996**, *26*, 481.

(29) (a) Bates, R. W.; Hanson, R. K.; Bowman, C. T.; Golden, D. M. *Abstract, First Joint Meeting of the U.S. Sections of the Combustion Institute*, George Washington University, Washington, DC, March, 14−17, 1999; p 629. (b) Bates, R. W.; Golden, D. M.; Hanson, R. K.; Bowman, C. T. *Phys. Chem. Chem. Phys.* **2001**, *3*, 2337.

(30) Hirschfelder, J. O.; Curtiss, C. F.; Bird, R. B. *Molecular Theory of Gases and Liquids*; Wiley: New York, 1966.

(31) Durant, J. L.; Kaufman, F. *Chem. Phys. Lett.* **1987**, *142*, 246.

(32) Kumaran, S. S.; Su, M.-C.; Lim, K. P.; Michael, J. V.; Wagner, A. F.; Harding, L. B.; Dixon, D. A. *J. Phys. Chem.* **1996**, *100*, 7541. Michael, J. V. *Combust. Sci. and Technol.* **1998**, *134*, 31.

(33) Dobbyn, A. J.; Stumpf, M.; Keller, H.-M.; Schinke, R. *J. Chem. Phys.* **1995**, *103*, 9947.

(34) Pastrana, M. R.; Quintales, L. A. M.; Brandão, J.; Varandas, A. J. C. *J. Chem. Phys.* **1990**, *94*, 8073.

(35) Litorja, M.; Ruscic, B. *J. Electron Spectrosc.* **1998**, *97*, 131.
(36) Whitten, G. Z.; Rabinovitch, B. S. *J. Chem. Phys.* **1963**, *38*, 2466; **1964**, *41*, 1883.
(37) Harding, L. B.; Troe, J.; Ushakov, V. G. *Phys. Chem. Chem. Phys.* **2000**, *2*, 632.
(38) Harding, L. B. Private communication, June 2000.
(39) Waage, E. V.; Rabinovitch, B. S. *Chem. Rev.* **1970**, *70*, 377.
(40) Bzowski, J.; Kestin, J.; Mason, E. A.; Uribe, F. J. *J. Phys. Chem. Ref. Data* **1990**, *19*, 1179.
(41) Paul, P. H. DRFM: A New Package for the Evaluation of Gas-Phase-Transport Properties. Sandia Report, SAND98-8203, November 1997.
(42) Hippler, H.; Siefke, M.; Stark, H.; Troe, J. *Phys. Chem. Chem. Phys.* **1999**, *1*, 57.
(43) Paul, P.; Warnatz, J. *Proc. Combust. Inst.* **1998**, *27*, 495.
(44) Ahumada, J. J.; Michael, J. V.; Osborne, D. T. *J. Chem. Phys.* **1972**, *57*, 3736.
(45) Lynch, K. P.; Schwab, T. C.; Michael, J. V. *Int. J. Chem. Kinet.* **1976**, *8*, 651.
(46) Michael, J. V.; Payne, W. A.; Whytock, D. A. *J. Chem. Phys.* **1976**, *65*, 4830.
(47) For the $Ne-H_2O$ van der Waals interaction, see Bagno, A. *J. Chem. Soc., Faraday Trans.* **1998**, *94*, 2501.
(48) For the $Ar-H_2O$ van der Waals interaction, see: Cohen, R. C.; Saykally, R. J. *J. Chem. Phys.* **1993**, *98*, 6007.
(49) For the $Kr-H_2O$ van der Waals interaction, see: van Wijngaarden, J.; Jager, W. *Mol. Phys.* **2000**, *98*, 1575.
(50) For the H_2-H_2O van der Waals interaction, see: Phillips, T. R.; Maluendes, S.; McLean, A. D.; Green, S. *J. Chem. Phys.* **1994**, *101*, 5824. Weida, J. J.; Nesbitt, D. J. *J. Chem. Phys.* **1999**, **110**, 156.
(51) For the O_2-H_2O van der Waals interaction, see: Svishchev, I. M.; Boyd, R. J. *J. Phys. Chem. A* **1998**, *102*, 7294.
(52) For the N_2-H_2O van der Waals interaction, see: Sadlej, J.; Rowland, B.; Devlin, J. P.; Buch, V. *J. Chem. Phys.* **1995**, *102*, 4804. Leung, H. O.; Marshall, M. D.; Suenram, R. D.; Ovas, F. J. *J. Chem. Phys.* **1989**, *90*, 700.
(53) For the CH_4-H_2O van der Waals interaction, see: Szczesniak, M. M.; Chalasinski, G.; Cybulski, S. M.; Cieplak, P. *J. Chem. Phys.* **1993**, *98*, 3078. Suenram, R. B.; Fraser, G. T.; Lovas, F. J.; Kawashima, Y. *J. Chem. Phys.* **1994**, *101*, 7230.
(54) For the H_2O-H_2O van der Waals interaction, see: Mas, E. M.; Bukowski, R.; Szalewicz, K.; Groenenboom, G. C.; Wormer, P. E. S.; van der Avoird, A. *J. Chem. Phys.* **2000**, *113*, 6687.
(55) Lendvay, G. *Z. Phys. Chem.* **2001**, *215*, 377.
(56) Dykstra, C. E. *J. Am. Chem. Soc.* **1989**, *111*, 6168.
(57) Bundgen, P.; Grein, F.; Thakkar, A. J. *J. Mol. Struct. (THEOCHEM)* **1995**, *334*, 7.
(58) Halkier, A.; Corinani, S.; Jorgensen, P. *Chem. Phys. Lett.* **1998**, *294*, 292.
(59) *CRC Handbook of Chemistry and Physics*, 80th ed.; Lide, D., Ed.; CRC Press: New York, 2000.
(60) Calaminici, P.; Jug, K.; Koster, A. M. *J. Chem. Phys.* **1998**, *109*, 7756.
(61) Harding, L. Private communication. The calculations used a correlation consistent triple-ζ basis set in a multireference singles and doubles configuration interaction electronic structure calculation.
(62) For He, there apparently is no information in the literature on either the $He-H_2O$ or $He-HO_2$ van der Waals complexes. Consequently, there is no information on r_e. In panel b, the r_e for the $Ne-H_2O$ van der Waals complex was used instead.
(63) Brunning, J.; Derbyshire, D. W.; Smith, I. W. M.; Williams, M. D. *J. Chem. Soc.* **1988**, *84*, 105.
(64) Kudla, K.; Schatz, G. C.; Wagner, A. F. *J. Chem. Phys.* **1991**, *95*, 1635.
(65) Wardlaw, D. M.; Marcus, R. A. *Chem. Phys. Lett.* **1984**, *110*, 230; Robertson, S. H.; Wagner, A. F.; Wardlaw, D. M. *J. Chem. Phys.* **2000**, *113*, 2648.
(66) Robertson, S. H.; Wagner, A. F.; Wardlaw, D. M. *J. Chem. Phys.* **1995**, *103*, 2917.
(67) Klippenstein, S. J.; Wagner, A. F.; Robertson, S. H.; Dunbar, R.; Wardlaw, D. M. VariFlex software, version 1.0, 1999. This software is available at no charge; see the VariFlex web site (*http://chemistry.anl.gov/chem-dyn/variflex*) for instructions on downloading and installation.
(68) Lendvay, G.; Schatz, G. C. *J. Phys. Chem.* **1992**, *96*, 3752.
(69) Lendvay, G.; Schatz, G. C. *J. Chem. Phys.* **1992**, *96*, 4356. Lendvay, G.; Schatz, G. C. *J. Phys. Chem.* **1991**, *95*, 8748. Lendvay, G.; Schatz, G. C. *J. Phys. Chem.* **1988**, *92*, 7223.
(70) Brown, N. J.; Miller, J. A. *J. Chem. Phys.* **1984**, *80*, 5568.
(71) Scoles, G. *Annu. Rev. Phys. Chem.* **1980**, *31*, 81.
(72) See for example: Atkinson, R.; Baulch, D. L.; Cox, R. A.; Hampson, R. F., Jr.; Kerr, J. A.; Troe, J. *J. Phys. Chem. Ref. Data* **1989**, *18*, 881.
(73) Hsu, K.-J.; Anderson, S. M.; Durant, J. L.; Kaufman, F. *J. Phys. Chem.* **1989**, *93*, 1018.
(74) Slack, M. W. *Combust. Flame* **1977**, *28*, 241.
(75) Campbell, I. M.; Rogerson, J. S.; Handy, B. J. *J. Chem. Soc., Faraday Trans. 1* **1978**, *74*, 2672.
(76) Mueller, M. A.; Yetter, R. A.; Dryer, F. L. *Proc. Combust. Inst.* **1998**, *27*, 177.
(77) Ashman, P. J.; Haynes, B. S. *Proc. Combust. Inst.* **1998**, *27*, 185.
(78) Kochubei, V. F.; Moin, F. B. *Soviet Prog. Chem. (Engl. Trans.)* **1973**, *39*, 29.
(79) Getzinger, R. W.; Schott, G. L. *J. Chem. Phys.* **1965**, *43*, 3237.
(80) Pirraglia, A. N.; Michael, J. V.; Sutherland, J. W.; Klemm, R. B. *J. Phys. Chem.* **1989**, *93*, 282.
(81) Polik, W. F.; Guyer, D. R.; Moore, C. B. *J. Chem. Phys.* **1990**, *92*, 3453.
(82) Abramson, E.; Field, R. W.; Imre, D.; Innes, K. K.; Kinsey, J. L. *J. Chem. Phys.* **1985**, *83*, 453.
(83) Perry, D. S.; Bethardy, G. A.; Davis, M. J.; Go, J. *Faraday Discuss.* **1995**, *102*, 215.
(84) For example: Xue, B.; Han, J.; Dai, H.-L. *Phys. Rev. Lett.* **2000**, *84*, 2606. Michaels, C. A.; Flynn, G. W. *J. Chem. Phys.* **1997**, *106*, 3558. Hartland, G. V.; Qin, D.; Dai, H. L.; Chen, C. *J. Chem. Phys.* **1997**, *107*, 2890.